Addis Ababa University

College of Natural and Computational Sciences

School of Earth Sciences

APPLICATIONS OF GRAVITY AND MAGNETIC METHODS TO MAP SUBSURFACE STRUCTURES, CONTRIBUTING TO GROUND WATER FLOW IN THE BULBULA-ARSINEGELE RIFT CORRIDOR, CENTRAL MAIN ETHIOPIAN RIFT.

A THESIS SUBMITTED TO

THE SCHOOL OF GRADUATE STUDIES OF ADDIS ABABA UNIVERSITY IN PARTIAL FULFILLMENT OF THE REQUIREMENTS FOR THE DEGREE OF MASTER OF SCIENCE IN EXPLORATION GEOPHYSICS

BY

DURESA WOYEMA

ADDIS ABABA, Ethiopia

JUNE, 2018

ADDIS ABABA UNIVERSITY
SCHOOL OF GRADUATE STUDIES
SCHOOL OF EARTH SCEINCES

This is to certify that the thesis prepared by **Duresa Woyema**, entitled: **"Gravity and Magnetic investigations of the Bulbula-Arsinegele rift corridor, central Main Ethiopian Rift: with an implication subsurface structure contribute to ground water flow"** and submitted in partial fulfillment of the requirements for the degree of Master of Science in Applied Geophysics complies with the regulations of the university and meets the accepted standards with respect to originality and quality.

Approved by examining committee:	Signature	Date
Dr. Balemwal Atnafu (Head, School of Earth Sciences)	_____	_____
Dr. Abera Alemu (Advisor)	_____	_____
Dr. Ameha Atnafu	_____	_____
Prof. Tilahun Mamo Internal Examiner	_____	_____
Prof. Tenalem Ayenew External Examiner	_____	_____

DECLARATION

I, the undersigned, hereby declare that the thesis entitled with **"**entitled: **"Applications of Gravity and Magnetic investigations of the Bulbula-Arsinegele rift corridor, central Main Ethiopian Rift: with an implication subsurface structure contribute to ground water flow"** is my original work carried out under the supervision of Dr. Abera Alemu and Dr. Ameha Atnafu and has not presented to any university or institution for the award of any degree or diploma program and all sources of materials used for the thesis are duly acknowledged.

Name of the candidate	Signature	Date
Duresa Woyema	_____	_____

This is to certify that the above declaration made by the candidate is correct to the best of our knowledge and it has been submitted for examination with our approval as university advisors.

	Signature	Date
Dr. Abera Alemu (Advisor)	_____	_____
Dr. Ameha Atnafu (Co - Advisor)	_____	_____

ABSTRACT

Analysis of newly acquired magnetic and existing gravity data constrained by the existing geologic information is made in order to delineate and map the subsurface geologic structures contributing to groundwater flow within the Bulbula-Arsi Negele rift corridor. Data enhancement (filtering) techniques have been applied both to the observed gravity and magnetic data in order to highlight the anomaly components resulting from deeper and shallower sources. The compiled residual anomaly map and its derivatives (regional, residual maps) reveal that relatively positive values which coincide with the locations of the Aluto volcanic center, Munesa ridge and high density basalt, rhyolite intrusion and extrusion of the Shala caldera. Correspondingly, the compiled magnetic anomaly maps including its derivatives (regional and residual maps) revealed that the volcanic centers residing the Aluto and Shala volcanic center and the Munesa basalt, rhyolite intrusion and extrusion are associated with relatively high magnetic anomalies. Relatively low magnetic anomalies are associated with the sediment dominated around the shore of Lake Langano, Lake Abijata, Lake Shala and the surrounding of Bulbula and O'itu towns.

The horizontal gradient gravity map and tilt derivative magnetic map compiled for the study area have determined the existence of NE-SW and N-S lineated subsurface geologic structures (faults and fractures) that favor the flow of groundwater from Lake Langano towards Lake Abijita and Lake Shala.

This M.Sc. thesis research has shown that there are no east west lineated structures that favor the flow of groundwater from Lake Langano towards Munesa ridge. Hence, the direction of groundwater flow in the study area takes place from Lake Langano towards Lake Abijita and Lake Shala being controlled by the N-S and NE-SW oriented faults and fractures mapped in the study area.

Keywords*:* Lake Langano, Lake Abijata, Lake Shala, Aluto Caldera, Bouguer gravity anomaly, magnetic anomaly, ground water flow.

ACKNOWLEDGMENTS

Sincere by thank my Advisor, Dr. Abera Alemu, School of Earth Sciences, Addis Ababa University, Addis Ababa and Co-advisor, Dr. Ameha Atnafu, for their immense encouragement, professional advice, full guidance, scholarly and productive comments, and for all their continued and indispensable support. I express my deep gratitude to Addis Ababa University for sponsoring and giving all facilities starting from the beginning of the courses until the termination of the study. I also thank the Ethiopian Mapping Agency (EMA) for providing Topographic map of the study area.

My special thanks go to Mr. Haile and Mr. Haptamu Atoma for their incredible support and assistance in processing gravity and magnetic data using Geosoft OasisMontaj software and Arc GIS software manipulation respectively.

I am grateful to all graduate students of the geophysics stream for their discussion and encouragement for the success of this MSc thesis work.

Last, but not least, I would like to convey my deep sense of gratitude to my family members, and colleges for supporting and encouraging me to complete this work.

Table of Contents

LIST OF FIGURES

LIST OF ACRONYMS

2D	Two dimensional
3D	Three dimensional
AVC	Aluto volcanic center
BRZ	Broadly Rifted Zone
CMER	Central Main Ethiopian Rift
ER	Ethiopian Rift
EARS	East African Rift System
FFT	Fast Fourier Transform
GPTL	Goba-Bonga tectonic lineament
GPS	Geographic positioning system
GSE	Geological survey of Ethiopia
IGRF	International Geomagnetic Reference Field
IGSN	International Gravity Standardization Network
MER	Main Ethiopian Rift
msl	Mean sea level
nT	Nano Tesla
NE	North East
NE –SW	North East – South West
N - E	North – East
NNE	North North East
NW	North West
NW- SE	North West – South East
NNE – SSW	North North East – South South West
NNW	North – North –West
N – S	North – South
SDZFZ	Siliti Debre Zeit Fault Zone

SE	South East
SI	Structural Index
SSW	South South West
S –W	South – West
SW	South West
WFB	Wonji Fault Belt
YTVL	Yerer-Tullu wellel Volcano-tectonic lineament

CHAPTER ONE

INTRODUCTION

1.1. Background

Geophysical methods are used to determine the geological sequences and structures of subsurface geology and economic sources by the measurement of certain physical properties. Of these properties density and magnetic susceptibility are used to determine the geological sequences and subsurface geological structures. Since geophysical methods are indirect method, they are used to study the subsurface lithological units and economic resource like ground water and economic valuable minerals by a desire to reduce the risk of drilling dry holes and also a desire to offset the costs associated with poor well of these economic needed.

Today, the geophysicist also provides useful parameters for hydrogeological modeling of both new groundwater supplies and for the mapping of subsurface structures like (fault and fracture) that control the flow of groundwater.

In this study, primary and secondary data were compiled, reviewed, analyzed and interpreted. Obtaining the secondary data includes collection of previous geophysical data including Gravity data, Topographic and Geological map relevant to the study area. The primary data set includes newly acquired magnetic data from 07 – 22 January 2018.

In the present study, gravity and magnetic data have been compiled, processed and interpreted to examine the subsurface geological structures and groundwater flow in the Bulbula-Arsinegele rift Corridor. Further, based on the results of gravity and magnetic anomaly maps, this work attempts to describe the subsurface geological sequences, tectonic setting and geologic structures of the study area.

The study area is located in the Central Main Ethiopian rift (CMER). The area ranges in elevation between 2400 m and 1500 m above sea level.

1.2 Description of the study area

1.2.1 Location and accessibility

The study area which comprises the Bulbula-Arsinagele rift corridor is located in the Central main Ethiopian rift (CMER) at about 220 km south of Addis Ababa (Fig. 1.1). The study area covers an area of approximately 3,100 square km. Geographically the study area is bounded between $7^0$00'N - 7^0 45'N Latitude or 800,000-855,200 UTM and $38^0$25'E - $39^0$00'E Longitude or 430,000 – 495,000 UTM coordinates.

The study area can be accessed through the major asphalt road running from Addis Ababa to Shashemene. In addition, there are several dry-weather roads crossing the area. These include gravel roads passing from Bulbula to the Aluto geothermal base camp Site and those connecting the Goljota, Aje, Degaga, Kenchere and Munesa towns.

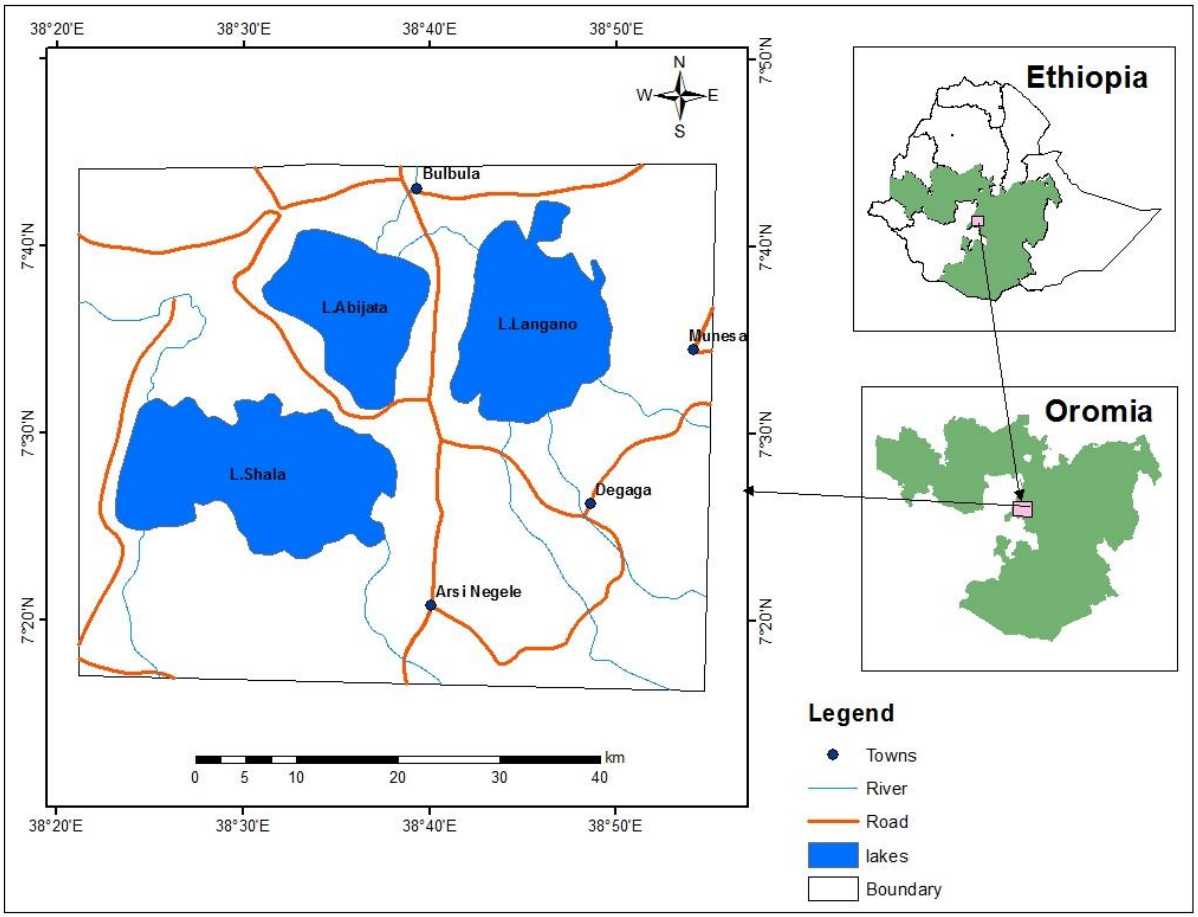

Figure 1.1 Location map of the study area

1.2.2 Physiography

The Ethiopian rift floor where the present study area lies rises in a rather irregular fashion from the Lake Rudolf basin to a maximum of over 1800m at the Dole town west of Lake Langano and east of Lake Abijata and then descends north wards in much more regular fashion in to the Afar depression, where the rift floor is below mean sea level. The average altitude of the plateaus on both sides of the rift is about 2600 m a.s.l. In general, the area is characterized by well-defined NNE – SSW structural blocks or units.

The topography of the corridors is dominantly covered by the rift floor of low altitude vary as 1570 meter above sea level (a.s.l) to 2300 m a.s.l and the western and eastern part of it, has small portion of rift escarpment and some part of high lands.

Existing mountains with in the corridors are Aluto plateau, Luga ridge, Abadir ridge & O'itu caldera which are concentrated on the Northern, southern and eastern part of the study area respectively. Relative to the western margins, the eastern rift margin is marked by deep gorges and canyons due to the existence of large regional marginal fault system.

The Rift floor in the eastern and southeastern of the Lake Abijata and Langano watershed is mainly covered by steep slopes characterized by abrupt faults. Its watershed is divided into three physiographic areas: the high plateaus on either side of the rift, the transitional escarpment and the rift floor (Makin, 1976). There is a topographic difference of about 2600 m between the rift floor and the highland areas (mountains).

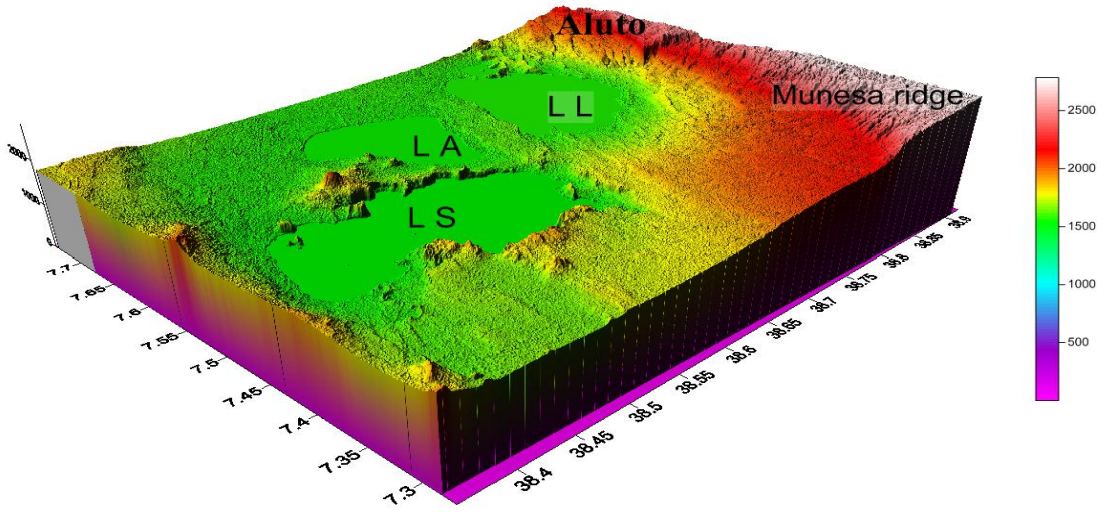

Fiure 1.2 Physiograpbic map of the study area

1.2.3 Drainage

Lake Abiyata is fed principally by Sade Sadin Rivers from its eastern sides and Lake Shala is fed by Hora Kalo from its northern side. Most parts of the plateau area are perennial sources of these rivers while the tributaries in the escarpments and rift floor are almost intermittent sources. The source for Hora Kalo is Lake Langano. In addition, the highland areas are characterized by higher drainage density than the escarpment due to differences in rock permeability, climate and slope (Dagnachew et al., 2004).

Sade river is one of the feeding rivers to the lake Abiyata on its south eastern part which raise from the munesa high land about 262 hectares of land is currently under cultivation using Sade River and its tributaries up stream of Sade town.

1.3. Statement of the Problem

Gravity and magnetic methods are thought to show the general structures of subsurface that contribute to the ground water flow and groundwater potential.

The ground water potential of the Bulbula-Arsinegele rift corridor is not studied using gravity and magnetic methods. This study is intended to contribute a solution for ground water problem in the specific location by using gravity and magnetic methods.

1.4. Basic Research Questions

The basic research questions of this MSc thesis may shortly be outlined as:

What are the major subsurface geologic structures that control groundwater flow in the study area?

How is the location of the major subsurface geologic structures mapped in the study area?

How is the depth and orientation of the mapped subsurface geologic structures estimated?

1.5. Objectives of the Study

1.5.1. General Objective

The main objective of the present work is to carry out gravity and magnetic investigations in the Bulbula-Arsinegele rift corridor of the CMER, with a view to map subsurface structures contributing to groundwater flow.

1.5.2. Specific Objectives

- Integrate the gravity and magnetic data with the existing geological and other relevant data for further interpretations.

- Map the major structures and identify subsurface weak zones that serve as a storage areas or conduits for groundwater movement.

- Establish a relationship between the gravity and magnetic with subsurface lineated geological structures and lithological units exposed on the surface.

- Map the locations, determine the orientations and estimate the possible depths of the major lineated geologic structures that control groundwater flow in the study area.

1.6. Expected Outcomes

The possible outcomes of this MSc research work that can be used by other researchers for future groundwater potential investigation in the study area can be stated as follows:

- A complete Bouguer gravity anomaly (CBA) map and its derivative maps of the study area.

- A total magnetic anomaly (TMA) map and its derivative maps of the study area.

- Location map of subsurface geologic structures controlling groundwater flow in the study area.

- Depth map of subsurface faults and fractures controlling groundwater flow in the study area.

1.7. Previous geophysical works and present study

Most of the gravity surveys carried out in the MER are regional in scale (e.g. Hunegnaw, 1989; Alemu, 1992). These regional surveys were conducted with the objective of investigating the crustal structure of the MER.

Several gravity investigations have been made in the CMER which consists of the present study area on a semi-regional and local scale (eg, Searl and Gouin, 1972; Alemu, 1983; Ayele, 2001; Saibi, 2012). The local gravity investigations were constrained by electrical resistivity data for the assessment of the geothermal potential associated with the Aluto and Corbetti volcanoes located in the CMER. The semi-regional gravity surveys were conducted with the objective of investigating the crustal structure and the subsurface geological and structural conditions beneath the CMER.

Gravity and magnetic investigations have been made in the CMER on a semi-regional and local scale (eg. Bekele et al., 2011; Berhane, 2015: Kelemework, 2016) for geothermal exploration and investigating the crustal structure including the subsurface geological and structural conditions in the CMER.

Loosely speaking, all the previous geophysical investigations did not consider application of the geophysical methods considered (gravity and magnetic) for groundwater investigations. However, the current study introduces a new interpretational approach using the new and the existing gravity and magnetic data to fulfil the cited objectives of this MSc thesis research.

1.8 Materials and methodology

1.8.1 Materials and software

For the present study the following materials and software have been utilized.

Topographic map with a scale of 1:50,000 was used during field survey. Several geological maps have been reviewed to know the surficial distribution of lithological and structural features, Google Earth online map to help to assess the overall setting of the study area before going to the field.

Proton precession magnetometer (MP-2) for magnetic data collection and hand held global positioning system (GPS) to determine the data location points.

Arc GIS 10.3 for the preparation of location and base map, Global mapper 12 to extrapolate and analyze gravity and magnetic data,

Geosoft oasis montaj for processing, and presenting the gravity and magnetic data employed in the research work.

1.8.2 Methodology

Any research project requires an appropriate and feasible methodology. Hence to achieve the general and specific objectives mentioned earlier the methodology involves three steps. These steps are classified as pre-field work, actual field work and post-field work.

1.8.2.1 Pre-field work

Identifying and reviewing of previous works relevant to the present work are very important and it was the first step in this study. Therefore the activities carried out in this step include;

Identification and interpretation of topographic maps, aerial photographs and geological maps

Literature review on geological and tectonic setting of the study area and the MER in general

Identifying and reviewing of relevant previous geophysical works (gravity and magnetic) has been made.

Obtain the available secondary data (gravity and magnetic) in the area for re-processing using the latest processing techniques available.

1.8.2.2 Actual field work

Field work was one of the most practical application of this study have been conducted. Under this work all the necessary primary geological and geophysical data have been collected as follows;

Acquisitions of magnetic data using a proton precision magnetometer have been carried out to fill the existing gaps in magnetic data coverage of the study area.

The magnetic data were collected randomly with average station spacing of 2-4 Km depending on the objectives, accessibility and field geological conditions.

The magnetic data were collected by establishing a base station and at each station magnetometer reading, time and elevation were recorded. Each base station was recovered (revisited) every 2 or 3 hours to determine diurnal variation.

Field observations on selected geological and structural features have been made.

1.8.2.3 Post field work

The primary data collected during field work and available secondary data have been processed and re-processed using different software packages. This software's include Geo-Soft, Arc GIS, and global mapper. Then the results present in the form of geophysical anomaly maps and profiles. Finally, the result has been qualitatively and quantitatively interpreted and correlated with previous works to produce probable subsurface structures contributing to ground water flow in the study area. The general frame work of the study is summarized by a flowchart (Fig.1.2).

1.9. Structure of the thesis

This thesis work is organized into six chapters. The first chapter deals with the general background, introduces the general frame work of the application of integrated geophysical methods to map the subsurface structures contributing for ground water flow. Specifically, it introduces the location and physiography of the study area, it explains the problem of statement of the study and the associated research questions formulated to solve the problem. This chapter also includes the general and specific objective of the study, its contribution to the scientific world and the methodology adopted to solve the problem and the materials utilized. Further, it briefly justifies the previous geophysical works conducted in the study area and main Ethiopian Rift as a whole. Finally, it indicates the limitations encountered and the overall structure of the thesis. The second chapter deals with the geologic and tectonic setting of the study area. Chapter three considers a theoretical background of the geophysical methods used in the study. The fourth chapter deals with the instrumentation, the data acquisition, reduction, processing, and presentation aspects the geophysical employed in this thesis work. In addition, the different filtering and data enhancement techniques used in this work are briefly discussed. Chapter five considers a discussion and interpretations of end results the geophysical surveys. In chapter six, conclusions and recommendations regarding the results of the MSc thesis research are outlined. Lastly, list of references in an alphabetical order based on the Addis Ababa University /sinet journal format are presented.

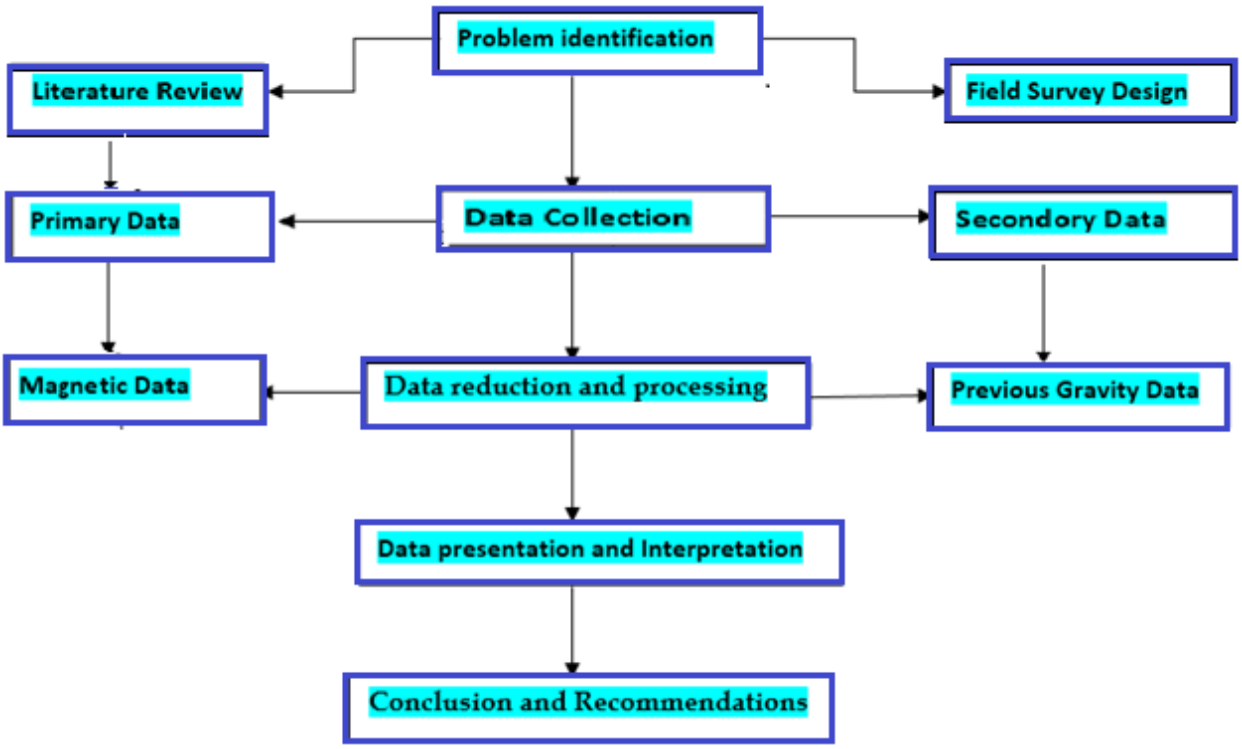

Figure 1.3 Flow chart showing the general frame work of the study

CHAPTER TWO

GEOLOGIC AND TECTONIC SETTING

2.1 Regional geology and tectonic setting

According to Corti (2009), the Ethiopian rift (ER) system is part of the East African Rift System (EARS) which comprises a series of rift zones extending over a distance of about 1000 km from the Afar triple junction at Red Sea–Gulf of Aden intersection to the Kenya Rift (KR) (Fig 2.1, Inset). The Ethiopian rift (ER) system consists of three major rift zones with distinct volcano-tectonic characteristics. These are the Afar rift, the Main Ethiopian Rift (MER) and the broadly rifted zone (BRZ) of southwestern Ethiopia (Corti, 2009) (Fig.2.1, Inset).

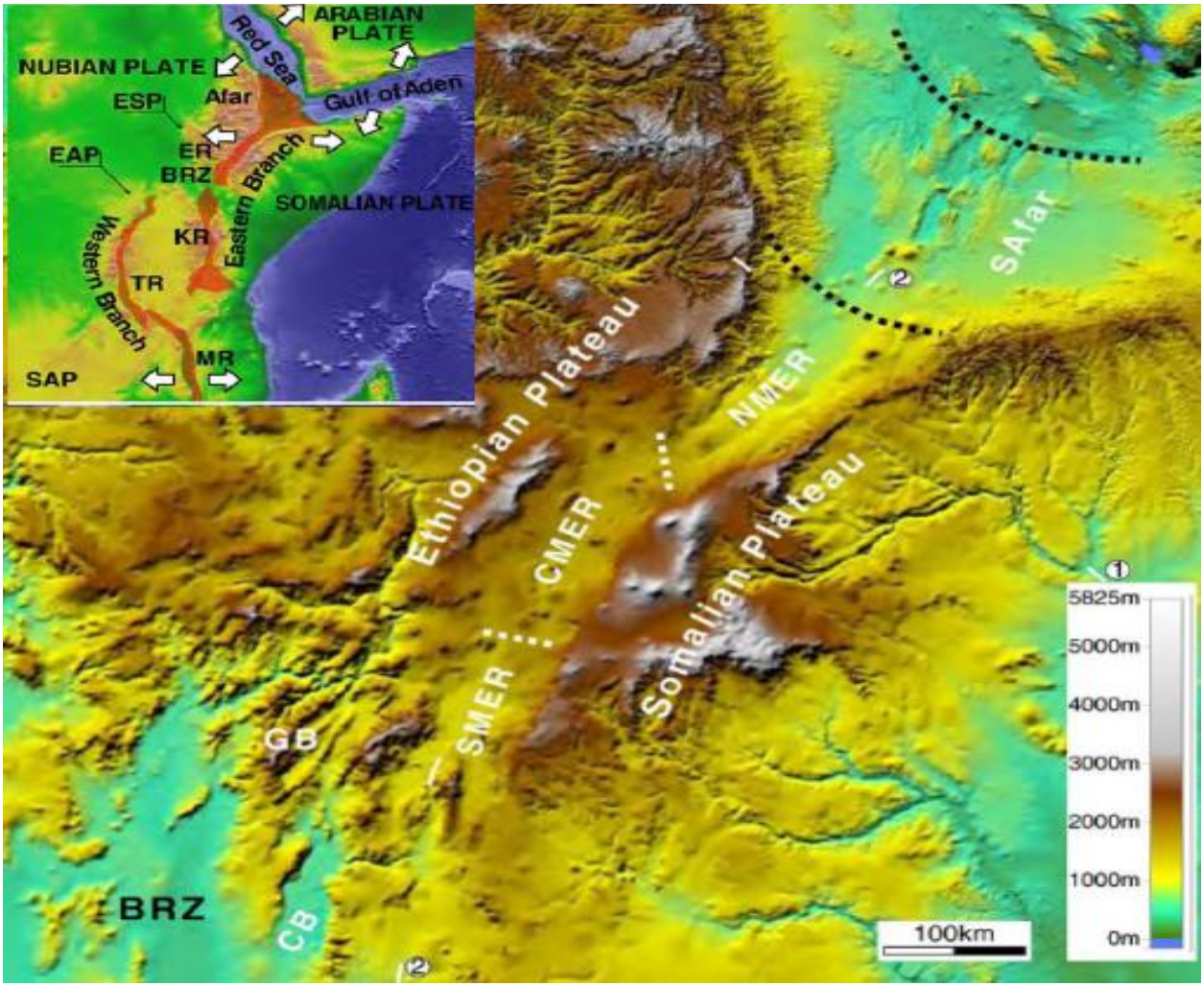

Figure 2.1 Map of Ethiopian rift showing the main rift segments Modified from Corti, 2009. Digital elevation model (SRTM data) of the Ethiopian Rift showing the main rift segments: (from north to south) Southern Afar (Safar), Northern Main Ethiopian Rift (NMER), Central Main Ethiopian Rift (CMER) and Southern Main Ethiopian Rift (SMER). BRZ: Broadly Rifted Zone; CB: Chow Bahir Rift; GB: Gofa Basin and Range.

Initiation of the Main Ethiopian Rift and the Afar rift can be traced back to 14 Ma (Kazmin and Habtemichael, 1978). Two main tectonic events have been recognized concerning the tectonic evolution of the Ethiopian Rift System. The first event that started since Eocene (Mohr, 1976a) involved the uplift of the Ethiopian swell. Large scale faulting later took place across the swell to form the Afar and the Main Ethiopian Rift which this represents the second major tectonic event. The last major episode of rift faulting resulted in the formation of a persistent belt of intense faults termed as the Wonji Fault Belt (WFB) by Mohr (1960). The WFB is thought to have shattered the rift floor into several relatively small horst and graben like structures all along the rift axis (Fig. 2.2).

The Main Ethiopian Rift (MER) is a symmetrical graben with uplifted flanks and steep border faults (Gidey et al, 1990). This structural depression serves as a divide between the Ethiopian Plateau (Northwestern Plateau) and Somalian Plateau (or Southeastern Plateau) (Fig. 2.1). The MER is believed to be the result of tensional movements that affected the uplifted Ethio-Somalia plateau (Di Paola, 1992; Mohr, 1986). A large number of normal faults have produced a total difference in altitude of more than 1000 m between the top of the plateau and the rift floor.

The Main Ethiopian Rift is a magmatic rift that recorded all the different stages of rift evolution from rift initiation to break up and incipient oceanic spreading (Ebinger, 2005; Corti, 2009). The MER is geographically subdivided into three sectors: Northern Main Ethiopian rift (NMER), Central Main Ethiopian rift (CMER) and Southern Main Ethiopian rift (SMER) (Gidey et al, 1990) (Fig. 2.1). The NMER extends from the MER–Afar boundary southwards to Lake Koka area, where it is separated from the CMER by the Boru Toru structural high (Bonini et al., 2005). To the south, the boundary between the CMER and the SMER can be placed at ~7° N around Lake Awasa area, where the rift margin rotates from NE–SW to N–S (Bonini et al., 2005). Width of the MER increases from the SMER (30-60 km) to the CMER (65-90 km) and the NMER (80-120 km) sectors, and is more than 200 km wide in southern part of the Afar Rift.

The present study area is located in the tectonically active CMER which is bounded by the Yerer-Tulluwellel volcano-tectonic lineament (YTVL) to the north and the Goba–Bonga tectonic lineament (GBTL) to the south (Fig. 2.2). In the study area, the CMER is bounded by the Munesa fault escarpment (a major rift border fault) to the east and the Guraghe escarpment (a major rift border fault) to the west of the rift floor.

Four lakes namely Lake Ziway, Abjata, Langano and Shala which are believed to have been formed by volcano-tectonic processes occupy the CMER (Fig. 2.1). As a result of differences in Abjata and Langano have an elongated shape parallel to the main trend of the CMER which indicates that they can be defined as tectonically controlled lakes. Unlike the three, Lake Shala occupies a caldera with its western part lying in a tectonically controlled depression which indicates that Lake Shala can be classified as a volcano-tectonically controlled deepest (≈250 m) lake. Lake Shala is thus identified to form a caldera (a high density magmatic center) known as the Shalla caldera or the O'A caldera with its local name (Mohr, 1960). O'A means hot and the name O'A caldera is derived from the abundant hot springs available around Lake Shale.

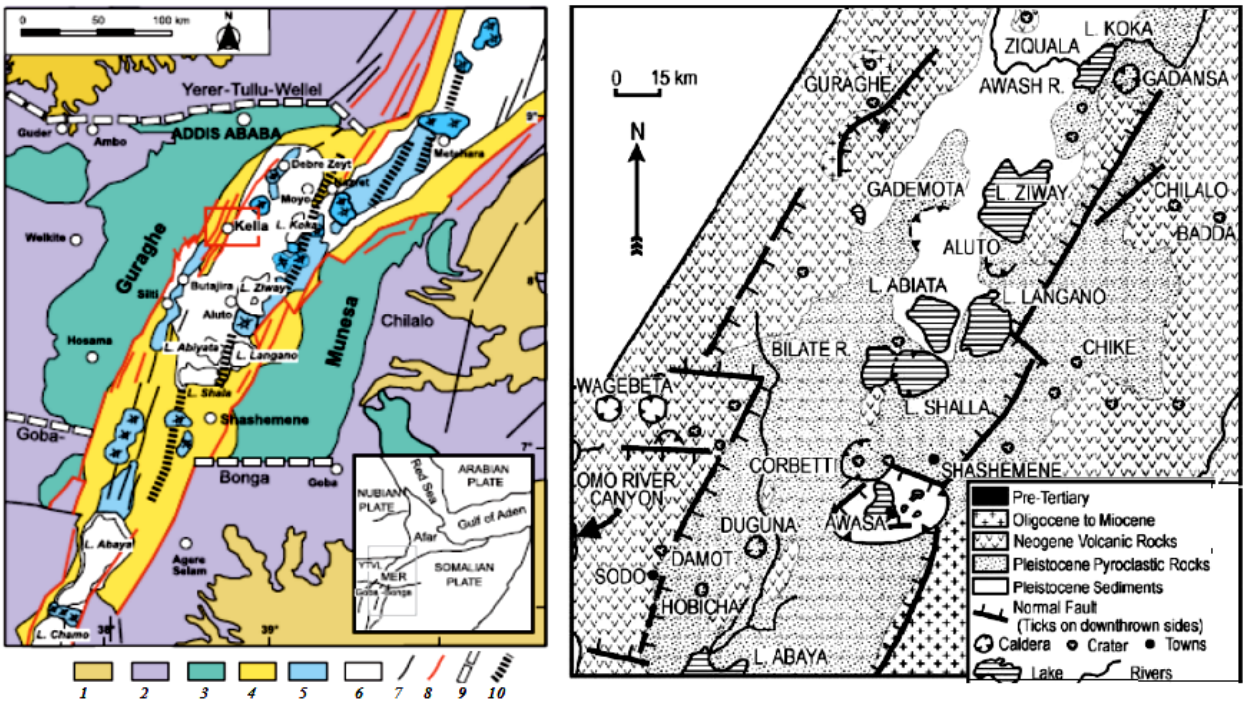

Figure 2. 1 Simplified geological and structural map of central Ethiopia (after Tsegay Abebe et al., 2010).
(1) Pre-Tertiary sediments and crystalline basement (2) Oligocene (32–29 Ma) and lower Miocene (12–8 Ma) plateau volcanics (3) Miocene–Pliocene rift shoulder trachytic–rhyolitic volcanics and pyroclastic layers (4) Plio-Pleistocene rift floor (5) Quaternary central volcanics and basaltic lava flows associated with phreato-magmatic deposits (6) Quaternary lacustrine sediments and interbedded pyroclastics (7) faults (8) rift border faults (9) major transversal tectonic lineaments in the basement (10) Wonji Fault Belt segments. In the inset: YTVL, Yerer-Tullu-Wellel volcano-tectonic lineament.

2.3 Geology and structural setting of the study area

The lithological units that make up the geology of the study area observed on the geologic map (Fig. 2.3) consist of late tertiary silicic volcanics (Aluto volcanic center) overlain by a unit of fissural flood basalt and Obsidian flows. The last major event of rift faulting which occurred in the quaternary age has resulted in the formation of so many volcanic complexes called the Munesa fault group in the eastern part of Lake Langano. The youngest stratigraphic succession of the study area is the Pleistocene-Holocene age lacustrine sediments which constitute the

central and northern parts of the study area and most part of the rift floor. In the study area the normal faults that are oriented NS parallel to the rift are visible cross-cutting the NE major fault system, forming small rhombic terrains in the south-eastern parts of the Aluto volcanic center, in particular between Munesa and Aluto and to a minor extent in its south-central and northern parts. The south-central NW faults cross Aluto diagonally and connect several important hydrothermal manifestations, such as: Kore – Finkilo (near Jawe Artu), Oitu Artu – Adonsha.

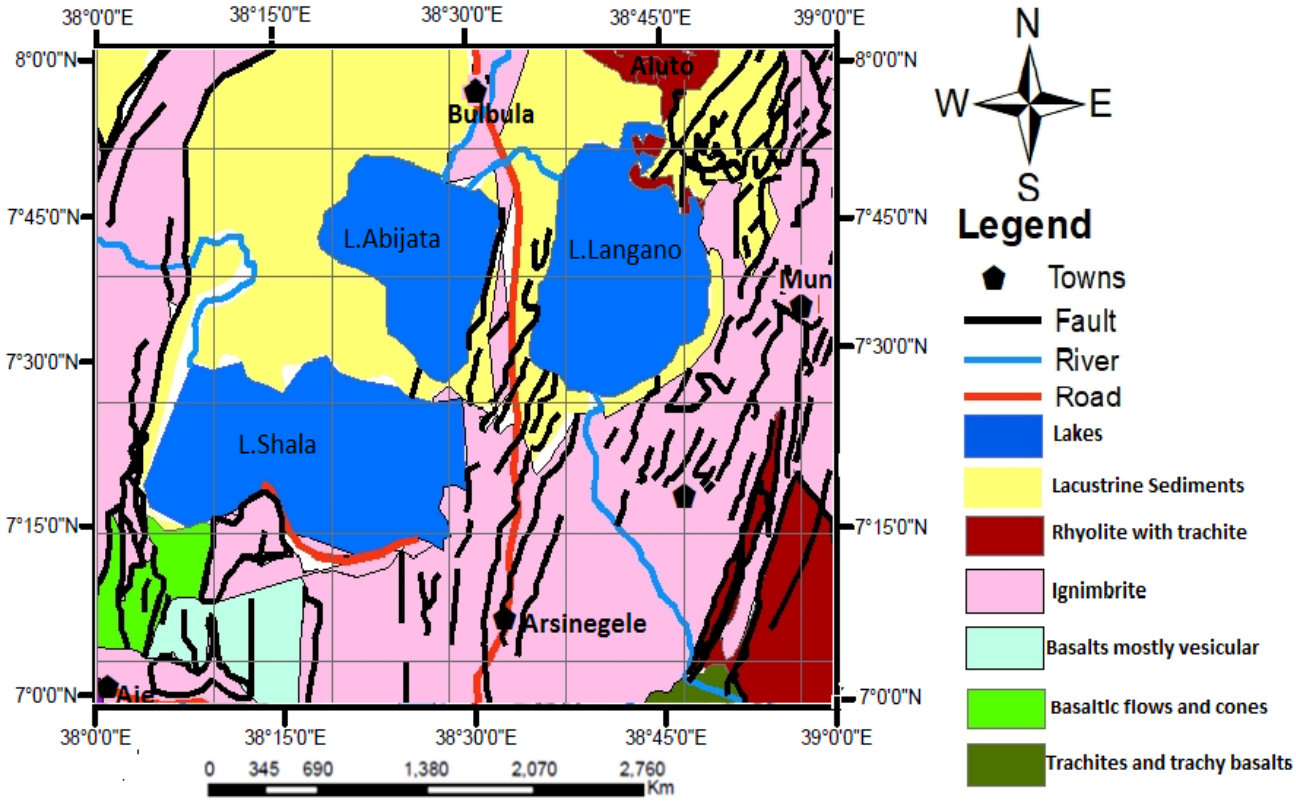

Figure 2. 2 Geologic map of the Bulbula-Arsinegele rift corridor modified from (EIGS 1975-76)

Some volcanic centers on the rift margin and within the rift itself follow the ENE trend, but are not as important as the NW-SE trend. The Aluto caldera follows the same trend. Moreover, the southern rim of the caldera is made up of a chain of volcanic centers' and craters that are elongated and aligned in an E-W direction.

In the study area the NE-SW trending faults and tectonic features are mainly expressed in the eastern and SE sectors and most of them deviate towards N, forming the NNE. Some of the volcanic centers, including the youngest three centers situated in the north-western part of the caldera, follow a NESW trend. This system has contributed significantly to the external and internal structural configuration of AVC. One of the important considerations refers to the fact that the older rock units, such as the Munesa crystal ignimbrite and the overlying Bofa basalt

outcropping in the eastern side, are gradually lowered down to the west and in the central part of the AVC these units are found at a depth of several hundred meters.

2.3.1 Rhyolite with some trachyte lava flows, pumice and unwelded tuffs

Most of the central volcanoes of the Aluto and Shala group are disposed along the axial zone of the rift in the study area. The main volcanic centers from north to south within the study area include the Aluto and Shala volcanic complexes. The main rock types associated with these volcanic complexes are rhyolitic and trachytic lava flows which tend to have higher densities as compared to lacustrine deposites of the rift floor

In some centers alkaline and per-alkaline products are mainly represented by pumice and unwelded tuffs. The sequence of eruption of various rocks differs from one volcano to another. Most of the products of central volcanoes are peralkaline rhyolites and trachytes of pantelleritic (Di Paola, 1976. and Tsegaye et al., 2005).

2.3.2 Pleistocene basalts mostly vesicular

Another type of volcanic activity in the Shala Group was the eruption from fissures of Pleistocene basalts. The bulk of these late basalts are concentrated in the southwestern part of Lake Shala (Fig.2.3).

2.3.3 Lacustrine Sediments, silts, clays, diatomite

Quaternary sediments mostly lacustrine origin is intercalated with Pliocene to Pleistocene ignimbrites both in the rift floor and rift shoulders. In the study area, the lacustrine sediments are dominant around the lakes Abijita, Shala, Langano and the rift floor north of their location (Fig.2.3). The major components of the sediments are volcanic origin, such as pumice and volcanic ash, obsidian, rhyolite and basaltic rock fragments (Tsegaye et al., 2005). Moreover, the overall density and magnetic susceptibility of the lacustrine sediments are thought to be lower than those of the volcanic rocks mapped on the geologic map (Fig.2.3) of the study area and the CMER (Fig. 2.2)

Basalts of the rift floor: These basalts are exposed at East of lake Langano and far North East of lake Abijata near Mito town (EIGS, 2012). The basalts are clearly controlled by extensional fractures and generally display fresh aa surfaces with chains of coriaceous cones.

Central volcanic complexes: According to EIGS (2012) most of the central volcanoes of the Wonji group are disposed along the axial zone of the rift, the WFB. The main volcanic centers with in the rift are the Aluto and O'a volcanoes. These volcanic complexes generally comprise rhyolitic and trachytic lava flows, ignimbrites, pumice, unwelded tuffs and obsidians.

2.3.4. Quaternary sediments

Quaternary sediments are the youngest units in the study area and constitute volcano sedimentary rocks and lacustrine sediments. As explained by Kazmin et al. (1980) lacustrine sediments intercalated with volcanics mainly ashes and tuffs, which in places are extensively developed and the sequence is shown as volcano-sedimentary which covers large area at the east of Shone town.

Numerous large lakes occupy the present day floor of the central Main Ethiopian Rift. A flat floor of red, yellow and white sands, tuffs, clays and diatomite are the common sediments in the lakes of Ziway, Langano and Abijata and indicates these lakes were all joined as one huge lake during the pluvials (Mohr, 1971). Hence, Pleistocene-Holocene lacustrine sediments cover a significant tract of ground and were deposited in a huge lake whose level before 3500 to 2100 years used to be 100m higher than its current level (Kazmin et al., 1980). The lacustrine sediments which are dominated by sand and silt are intercalated with re-deposited volcanic ash and tuffs (EIGS, 2012). The main components of the derived sediments are volcanic origin, such as pumice and volcanic ash, obsidian, rhyolite and basaltic rock fragments.

CHAPTER THREE

THEORY OF THE GEOPHYSICAL METHODS

3.1. Gravity Method

3.1.1. Introduction

According to Lillie (1999), gravity is derived from Greek word "gravis", which means heavy and it is defined as the force of attraction between masses or it is the force of attraction that tends to draw bodies in Earth's sphere towards the center of the Earth. The gravity method is one of the potential field methods that measures variations in Earth's gravitational field in the given study area. In applied geophysics, gravity surveying is conducted to investigate the subsurface geology based on variations in the Earth's gravitational field caused by difference in density between rocks beneath the Earth's surface. The gravitational attraction of a body of non-homogenous density will vary from one measuring point to another due to difference in the distribution of density in the body. These variations in gravitational attraction of the Earth from point to point will provide valuable information about the subsurface geology.

3.1.2. Basic principles of gravity

The basis for the gravity method is Newton's universal law of gravitation which states that the attraction force between two point masses m_1 and m_2, separated by a distance "r" is given by:

$$\mathbf{F = G\frac{m_1 m_2}{r^2}} \qquad (3.1)$$

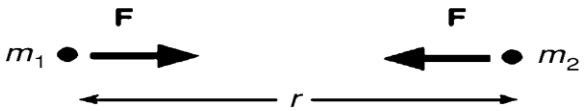

Where F = Force of attraction between the two objects (N), G = Universal gravitational constant (6.67×10^{-11} Nm^2kg^{-2}), m_1m_2 = Product of the masses of the two objects in kg and r = Distance between the two masses. The force (F) exerted on the object of m_1 by the body with mass m_2, is given by Newton's second law of motion:

$$F = m_1 a \qquad (3.2)$$

Where a = acceleration of object mass m_1, due to the gravitational attraction of the object mass m_2 (m/s^2). Solving for acceleration, in equation (3.2) we get:

$$\mathbf{a = \frac{F}{m_1}} \qquad (3.3)$$

Substituting $F = G\frac{m_1 m_2}{r^2}$ from equation (3.1) in equation (3.3) give:

$$\mathbf{a = \frac{F}{m_1}} = \mathbf{G\frac{m_2}{r^2}} \qquad (3.4)$$

For Earth's gravity field $a = g$ = Gravitational acceleration observed on or above the Earth's surface with $m_2 = Me$ = Earth's mass and $r = R$ = Distance from the observation point to the Earth's center of mass so that:

$$\mathbf{g = \frac{GM}{R^2}} \qquad (3.5)$$

Equation (3.5) illustrates two fundamental properties of gravity (Lillie, 1999):

Acceleration due to gravity doesn't depend on the mass (m_1) attracted to the Earth ,provided the mass is dropped in a vacuum)

The farther the object from the Earth's center of mass (that's the greater the radial distance), is the smaller the value of "g" and thus, gravity obeys an inverse square law.

3.1.3 Gravity units

In the cgs system, the unit of acceleration is cm/s^2, which is referred as gal, named after Galileo. The numerical value of g at the surface of the Earth is about 980 cm/s^2 (gals). In exploration work geophysicists are likely to be measuring differences in acceleration one-ten-millionth or less of the Earth's gravity field. This unit and its subdivisions commonly used by geophysicists are defined as,

1 gal = 1 cm/s^2

1 gal = 1000 milligals (mgal)

1 gal = 10,000 gravity units (g.u.)

1 gal = 1,000,000 micro gals (μgal)

The SI units of acceleration are, 1 m/s^2 = 10^2 gal = 10^5 mgal = 10^6 g.u. = 10^8 μgal

3.1.4 Gravity Reduction

For most geophysical methods, it is necessary to apply a variety of corrections to the raw data obtained in the field in order to reduce or prepare the data for further enhancement and interpretation (Dentith and Mudge, 2014)

In gravity method, more than in any other branch of geophysics, large and in principle calculable effects are produced by sources that are not of direct geological interest (Milsom and Eriksen, 2011). For example, the value of the observed gravity "g_{ob}"at a given observation point is affected by different factors such as the elevation above mean sea level where the point is located, the latitude in which the point is located, the topography of the area in which the measurement is taking place, etc. These effects are removed by corrections that involve the sequential calculation of a number of recognized quantities. In each case, a positive effect is one that increases the magnitude of the measured field and the sign of the reduction is opposite to that of the effect it is designed to remove (Milsom and Erikson, 2011). This process is known as gravity reduction (Kearey et al., 2002 as cited in La Fehr, 1991) or reduction to the geoid as the sea level is usually the most common datum level, although the datum plane need not necessarily be the mean sea level (Dobrin, 1988).

Although most corrections are spatial, some are to allow for factors that change the reading when the gravimeter is at the same location (Musset and Khan, 2000). Drift and Earth Tide correction types are time dependent; whereas the spatial type of corrections are related to variations in distance from the center of the Earth. Accordingly, first the time dependent corrections and then the space dependent corrections will be explained next.

3.1.4.1 Instrumental drift correction

The basis for instrumental drift correction arises from the fact that gravimeter reading change (drift) with time as a result of elastic creep in the springs, producing an apparent change in gravity at a given station (Reynolds, 1997). Correction for instrumental drift is thus, based on repeated readings at a base station at recorded times throughout the day (Kearey et al., 2002). The base station is commonly revisited at every 1-2 hours (Reynolds, 1997).

The differences between successive measurements at the same station are plotted to produce a drift curve and the observed gravity values from intervening stations can be corrected by subtracting the amount of drift from the observed value (Reynolds, 1997). Drift is assumed to be linear between consecutive base readings. (Kearey et al., 2002)

3.1.4.2 Tidal Drift correction

Tides are caused by variations in gravity observations resulting from the attraction of the celestial bodies (moon and sun). The Earth's body experiences an elastic deformation due to the tidal forces (Earth body tides) (Torge, 1989). The resulting bulges in the surface have diurnal periodicity which is predictable at any point on the surface of the Earth. The tidal variations can be on the range of 0.2 to 0.3 mgal (Dobrin, 1988). So using the full sensitivity of the gravimeter these variations must be removed.

3.1.4.3 Latitude correction

According to Telford et al. (1990) the latitude correction arises two effects: First, since the Earth rotates around its axis and this rotation tends to produce a centrifugal acceleration force which opposes the effect of the gravitational acceleration. This centrifugal acceleration is maximum at the equator and zero at the poles. Second, due to the imperfect spherical shape of the Earth (i.e. flattened at the poles and bulged at the equator), a variation in both equatorial and polar radii arise. This phenomenon gives rise to gravity value variation with distance from the center of the Earth. The latitude correction is thus applied in order to account for these two effects. The average value of gravity for a given latitude (θ) is approximated by the 1967 reference gravity formula, adopted by the International Association of Geodesy (Lillie, 1999).

$$g_t = g_e(1 + 0.005278895\sin^2\theta + 0.000023462\sin^4\theta) \quad (3.6)$$

Where g_t = Theoretical gravity for the latitude of the observation point (mgal)

g_e = Theoretical gravity at the equator (978031.85 mgal)

θ = Latitude of the Observation Point (Degrees)

3.1.4.4 Free air correction

Free air correction (FAC) starts from the concept of gravity which is inversely proportional with the square of distance from the center of the Earth. Hence, it is necessary to correct for changes in elevation between stations to reduce field readings to a datum surface (Telford et al., 1990).

It is the allowance for the reduction of the magnitude of gravity with height from the center of the Earth irrespective of the nature of the rock between the observation point and the center of the Earth (Reynolds, 1997; Telford et al., 1990).

The change in gravity (Δg) with increasing distance from the center of the Earth (ΔR) is given by the first derivative of g with respect to R (Lillie, 1999) as:

$$\lim_{\triangle Rappr0} = \frac{\triangle g}{\triangle R} = \frac{dg}{dR} = -\frac{2}{R}\frac{GM}{R^2} = \frac{-2}{R}\ g$$

$$\frac{dg}{dR} = \frac{-2g}{R}$$

Assuming average value of: $g = 980.625 mGal \ \& \ R = 6.367 km = 6367.000 m$

$$\mathbf{\frac{dg}{dR} = \frac{-2g}{R} = -0.308\ mGal/m} \qquad (3.7)$$

Where $\frac{dg}{dR}$ = Average value for the change in gravity with increasing elevation

The above equation (3.7) illustrates that for approximately every 3m upward from the surface of the Earth, the acceleration due to gravity decreases by about 1mgal (Lillie,1999).

3.1.4.5 Bouguer correction

Bouguer correction is made due to the variation of gravity data from station to station due to differences in mass between the observation point and the sea level datum (Lillie, 1999). The Bouguer correction (BC) is thus, to account for the attraction of material between the station and the datum plane that was ignored in the free air correction (Telford e al.,, 1990).

Bouguer correction is done by approximating the mass as an infinite slab, with thickness (h) equal to the elevation of the station (Lillie, 1999). The attraction of such slab is:

$$BC = 2\rho rGh \quad (3.8)$$

Where BC= Bouguer Correction

ρ= Density of the Slab

G= Universal gravitational Constant

h = Thickness of the slab

Substituting the values of G and 2ρ in equation (3.8) yields:

$$BC = 0.0419\rho h \quad (3.9)$$

Taking the average crustal density of 2.67 g/cm^3 and substituting it in the above Eq. (3.9) yields:

$$BC = 0.112(^{mGal}/_{m})h \quad (3.10)$$

It can be seen from equation (3.10) that, for every 9 meter of surface elevation, the increased mass below the observation point adds about 1mgal to the observed gravity. (Lillie,1999). The Bouguer correction is subtracted from the observed gravity value if the station is above the datum plane and is added when the station is below the sea level.

3.1.4.6 Terrain correction

The Bouguer correction assumes that the rock occupying the height interval between the datum level and the station is a uniform slab extending to infinity in all directions (Dentith and Mudge, 2014). In other words, the land surface is assumed to be represented by a subdued topography (i.e. the terrain around the observation point is perfectly flat). In reality, there exist "hills" (mountains) rising above the observation point and "valleys" below the observation point.

According to Telford et al., (1990), the terrain correction is thus, to allow for surface irregularities in the vicinity of the observation point. Hills above the elevation of the gravitation station exert an upward pull on the gravimeter, whereas valleys (lack of material) below it fail to pull down ward on it. Thus, both types of topographic undulations affect gravity measurements in the same sense as a result of which, the terrain correction is usually added to the observed gravity reading (e.g. Dobrin, 1988; Telford et al., 1990; Reynolds, 1997).

3.1.5 Gravity anomaly

Gravity observations can be used to interpret changes in mass below different regions of the Earth. To see the mass differences, the broad changes in gravity from equator to pole must be subtracted from station observations by predicting the gravity value for a station's latitude (theoretical gravity), then subtracting that value from the actual value at the station (Observed gravity), yielding a gravity anomaly (Lillie, 1999).

A discrepancy between the corrected, measured gravity and the theoretical gravity is called a gravity anomaly (Lowrie, 2007). It arises because the density of the Earth's interior is not homogeneous. The most common types of gravity anomalies are the Bouguer anomaly and the free-air anomaly.

3.1.5.1 Free air gravity anomaly

The free air gravity anomaly (ΔgF_A) takes in to account the latitudinal change in gravity on the Earth's best fitting ellipsoid represented by the theoretical gravity (g_t) and the vertical change in gravity between the reference datum and the observation height assuming that the gravity station is located in free air, hence the name free air anomaly (Hinze et al., 2013).

Lillie (1999) defined free air gravity anomaly as the observed gravity (g_{obs}) corrected for latitude and elevation of the station. The free air gravity anomaly is mathematically calculated as:

$$\Delta gF_A = g_{obs} + FAC - g_t \qquad (3.11)$$

Where ΔgF_A = Free air gravity anomaly; g_{obs} = Observed gravity; FAC = Free air correction and g_t = Theoretical Gravity

From equation (3.11), two things can be understood (Lillie, 1999):

Subtracting the theoretical gravity from the observed gravity corrects for the latitude, thus accounting for the spin and bulge of the Earth. Adding the "FAC" puts back the gravity lost to elevation, there by correcting the increased radius "R" from the Earth's center.

3.1.5.2 Bouguer gravity anomaly

The Bouguer gravity anomaly, like the free air gravity anomaly reflects changes in mass distribution below the surface, except the Bouguer anomaly has had an additional correction, removing the effect of mass above sea level datum on land (Lillie, 1999).

The Bouguer gravity anomaly is the most frequently used of the gravity anomalies in surveys of continental and in near shore marine areas (Hinze et al., 2013).

The variation of the Bouguer anomaly should reflect the lateral variation in density such that a high density feature in a lower density medium should give rise to a positive Bouguer anomaly. Conversely, a low density feature in a high density medium should result in a negative Bouguer anomaly (Reynolds, 1997). The simple Bouguer gravity anomaly (Δg_{Bs}) on land is computed from the free air gravity anomaly (Lillie, 1999).

$$\Delta g_{Bs} = \Delta gFA - (0.112\,{}^{mGal}\!/_{m})h \qquad (3.12)$$

Where h= the elevation in meters.

3.2 Magnetic method

3.2.1 Introduction

Magnetic and gravity methods have much in common, but magnetics is generally more complex and variations in the magnetic field are more erratic and localized (Telford et al., 1990). This is partly due to the difference between the dipolar magnetic field and the mono polar gravity field, and due to the variable direction of the magnetic field, whereas the gravity field is always in the vertical direction. In line with this, the magnetic field varies with time whereas gravity field is time invariant (ignoring small tidal variations).

The aim of a magnetic survey is to investigate subsurface geology on the basis of anomalies in the Earth's magnetic field resulting from the magnetic properties of rocks (Kearey et al., 2002).

3.2.2 Fundamental cconcepts of magnetic field

The theories of magnetic field are similar to that of electric and gravity in that, point magnetic poles are analogues to point electrical charges and point masses (Telford et al., 1990).

If two magnetic poles of strength p_1 and p_2 are separated by a distance "r", a force (F) exists between them. If the poles are of opposite in sign, the force is attractive and thus operating to move them towards each other, whereas if the poles are the same sign, the force is repulsive and operating to push them apart (Hinze et al., 2013).

Coulomb in the late 18 th century investigated experimentally the relationship between forces and the poles and this relationship was put mathematically by Poisson. Finally, the mathematical relationship came to be called "Coulomb's law and is given by (Hinze et al., 2013):

$$F = \mu p_1 p_2 / r^2 \qquad (3.13)$$

Where $p_1 and p_2$ = Point magnetic poles of strength "P", r = distance between them and μ = Magnetic permeability (measure of the ease with which the magnetic field is passed through the material separating the poles)

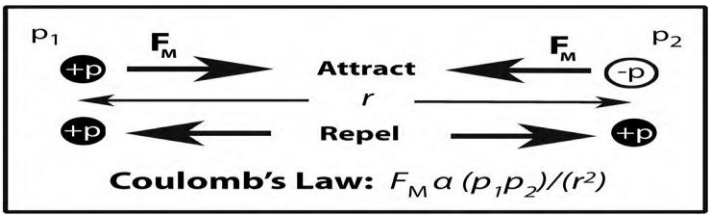

Schematic illustration of the attractive and repulsive magnetic forces generated between two magnetic poles by Coulomb's law (After Hinze et al., 2013)

3.2.3 The geomagnetic field

Geomagnetism refers to the study of magnetic phenomena exhibited by the Earth and its atmosphere. Although the existence of the geomagnetic field has been recognized for a very long period of time, it was not until 1843 that the variations in the field were used to locate deposits of magnetic ores (Telford et al., 1990). The magnetic field observed at the Earth's surface varies considerably both in direction and magnitude (Milsom, 2003).

3.2.3.1 Origin of Earth's magnetic field

Even though several theories have been developed to explain the origin of magnetic field of the Earth, the Magneto Hydrodynamic (MHD) theory seems to have received a fair acceptance.

According to this theory, the geomagnetic field is believed to be originated by the core field caused by rapid and complex flow of highly conductive, metallic iron in the outer core. The magnetic source is thought to be a self-excited dynamo in which highly conductive fluid moves in a complex manner caused by convection (Telford et al., 1990).

About 98% of the Earth's magnetic field is of internal origin, thought to be caused by motions of liquid metal in the core; the remaining 2% is external, of solar origin (Lillie, 1999).

3.2.3.2 Nature of Earth's magnetic field

Although there are several parts of the geomagnetic field of the Earth, the following three are important as far as exploration geophysics is concerned (Telford et al., 1990).

Main field: This field varies relatively slowly and is of internal origin.

A small field compared to the main field, it varies rapidly and originates outside of the Earth.

Spatial variations of the main field is usually smaller than the main field which is nearly constant in time and space. They are caused by local magnetic anomalies in the near surface crust of the Earth and are targets of magnetic surveying.

3.2.3.3 Temporal variations of Earth's magnetic field

The magnetic field of the Earth varies with time. As a result the temporal variation of the Earth's magnetic field can be explained in terms of three temporal variations.

Secular variations: These are very long period changes that result from convective changes in the core. They are monitored by measuring changes in I, D and B at observatories. Because these variations occur slowly with respect to the time of completion of a typical exploration magnetic survey, these variations will not complicate data reduction efforts.

Diurnal variations: Magnetic effects of external origin cause the geomagnetic field to vary on a daily basis to produce diurnal variations. Under normal conditions (quiet days) the diurnal variation is smooth and regular and has an amplitude of about 20–80nT, being at a maximum in Polar Regions (Kearey et al., 2002). This variation should be accounted for when conducting exploration magnetic surveys.

Magnetic storms: Occasionally, magnetic activity in the ionosphere will abruptly increase. The occurrence of such storms correlates with enhanced sunspot activity. The magnetic field

observed during such times is highly irregular and unpredictable, having amplitudes as large as 1000 nT. Exploration magnetic surveys should not be conducted during magnetic storms. This is because the variations in the field that they can produce are large, rapid, and spatially varying. Therefore, it is difficult to correct for them in acquired data (Kearey et al., 2002).

3.2.3.4 Elements of Earth's magnetic field

A vector that describes the magnetic field strength and direction from a give position can be broken in to its components:

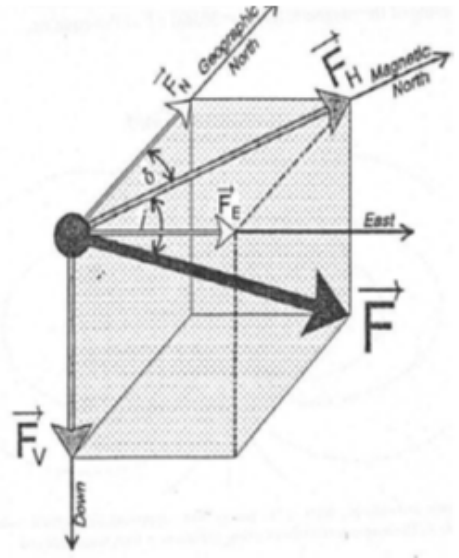

$\vec{F}$ = Total Magnetic Field Vector

$\vec{F_H}$ = Horizontal component of the total field vector

$\vec{F_V}$ = Vertical component of the field vector

$\vec{F_N}$ = North component of the horizontal vector

$\vec{F_E}$ = East component of the Horizontal vector

δ = Declination

Fig.3.1 Elements of Earth's magnetic field (After Lillie, 1999)

From the above figure, we can derive the following relations:

$$\vec{F}_H^{\,2} + \vec{F}_V^{\,2} = \vec{F}^2 \;;\; \vec{F} = \sqrt{F_N^{\,2} + F_V^{\,2}} = \sqrt{F_N^{\,2} + F_E^{\,2} + F_V^{\,2}} \;;\; \vec{F}_N^{\,2} + \vec{F}_E^{\,2} = \vec{F}_H^{\,2}$$

$$i = \tan^{-1}\left(\frac{F_V}{F_H}\right) \;;\; \delta = \tan^{-1}\left(\frac{F_E}{F_H}\right)$$

3.2.4 Magnetization and magnetic susceptibility of materials

3.2.4.1 Magnetization

If a body is placed in an external magnetic field (also called inducing field), it acquires although usually small, a magnetization which is proportional to the inducing field (Milsom, 2003). The relationship is given as:

$$\mathbf{M} \propto \mathbf{H} \qquad (3.14)$$

(The magnetization acquired is directly proportional to the induced field)

$$\mathbf{M} = \chi \mathbf{H} \qquad (3.15)$$

Where $M =$ Magnetization acquired by the material, $\chi =$ Magnetic susceptibility of the material and $H =$ Inducing field

3.2.4.2 Types of Magnetization

Magnetization of a rock occurs in two ways: Induced magnetization and Remnant Magnetization.

Induced Magnetization: This type of magnetization is acquired by materials only when the inducing field exists. The magnetization acquired decays rapidly when the inducing field is removed. Magnitude and direction of induced magnetization depends on the magnitude and direction of ambient field and on the susceptibility of the rock being magnetized. This part of the field is important in magnetic method of prospecting.

Remnant Magnetization: This type of magnetization is acquired by the material even if the ambient/ inducing field is removed. Remnant magnetization commonly occurs when rocks form from hot magma, in which the magnetic domains of some minerals behave as compass needles, orienting themselves in the direction of the ambient magnetic field existed at that time.

This part of magnetization is important in the study of paleomagnetism, in which the science has contributed much to our understanding of the ages of the rocks, the latitude at which they formed and the relative positions of continents in the past.

3.2.5 Magnetic instruments

Magnetic instruments basically used in geophysical exploration can be classified in to three groups: the torsion (and balance), fluxgate and resonance type's magnetometers.

Flux-gate magnetometer: The construction of this instrument involves two coils wound in opposition. A current is passed through to induce magnetization. A secondary winding measures the voltage induced by the induced magnetization. In the absence of the Earth's field these two cancel out. An AC current is applied that saturates the cores in opposition in the absence of the Earth's field. The Earth's field reinforces one core and opposes the other. This causes the

voltages induced in the secondary coils to get out of step. The result is a series of pips whose height is proportional to the ambient field (Foulger and Peirce, 1876).

Proton precession magnetometer: The most commonly used magnetometer for both survey work and observatory monitoring is currently the nuclear precession or proton magnetometer. The sensing device of the proton magnetometer is a container filled with a liquid rich in hydrogen atoms, such as kerosene or water, surrounded by a coil (Kearey et al., 2002). Field instruments provide absolute readings of the total magnetic field.

3.2.6. Magnetic surveying

Magnetic exploration can be carried out on land, at sea, and in the air.. Land surveys are usually done with portable proton precession magnetometers. Profiles or networks of points are measured in the same way as for gravity. This will give diurnal drift and detect magnetic storms (Foulger and Peirce, 1876). In magnetic surveying the operator must: record the time at which readings were taken for drift correction, stay away from interfering objects (e.g., wire fences, railway lines, roads), not carry metal objects (e.g., mobile phones), and take multiple readings at each station to check for repeatability.

3.2.7 Magnetic data reduction

To remove all causes of magnetic variation from the observations other than those arising from subsurface geology it is necessary to make correction of magnetic data.

Diurnal variation correction: The effects of diurnal variation may be removed in several ways. The differences observed in base readings are then distributed among the readings at stations occupied during the day according to the time of observation. Base readings are taken to correct for temporal variation in the measured field **(Kearey et al., 2002).**

Geomagnetic correction: In order to produce a magnetic anomaly map of a region, the data have to be corrected to take in to account the effect of latitude and to a lesser extent longitude (Reynolds, 1997). Survey data at any given location can be corrected by subtracting the theoretical field value B_{th}, obtained from the International Geomagnetic Reference Field (IGRF) from the measured value, B_{ob}. Therefore, the magnetic anomaly (ΔB), obtained by subtracting the diurnal correction (δB_D) and geomagnetic correction (B_{th}) is given by;

$$\Delta B = B_T - \delta B_D - B_{th} \qquad (3.16)$$

CHAPTER FOUR

DATA ACQUISITION, PROCESSING AND PRESENTATION

4.1 Gravity data acquisition and distribution

A total of about 574 gravity data with an average spacing of 2 to 4Km between consecutive stations has been obtained and used for this study. These points are randomly distributed along seasonal roads, dry weather roads (gravel and asphalt) and off road transect (Fig. 4.1).

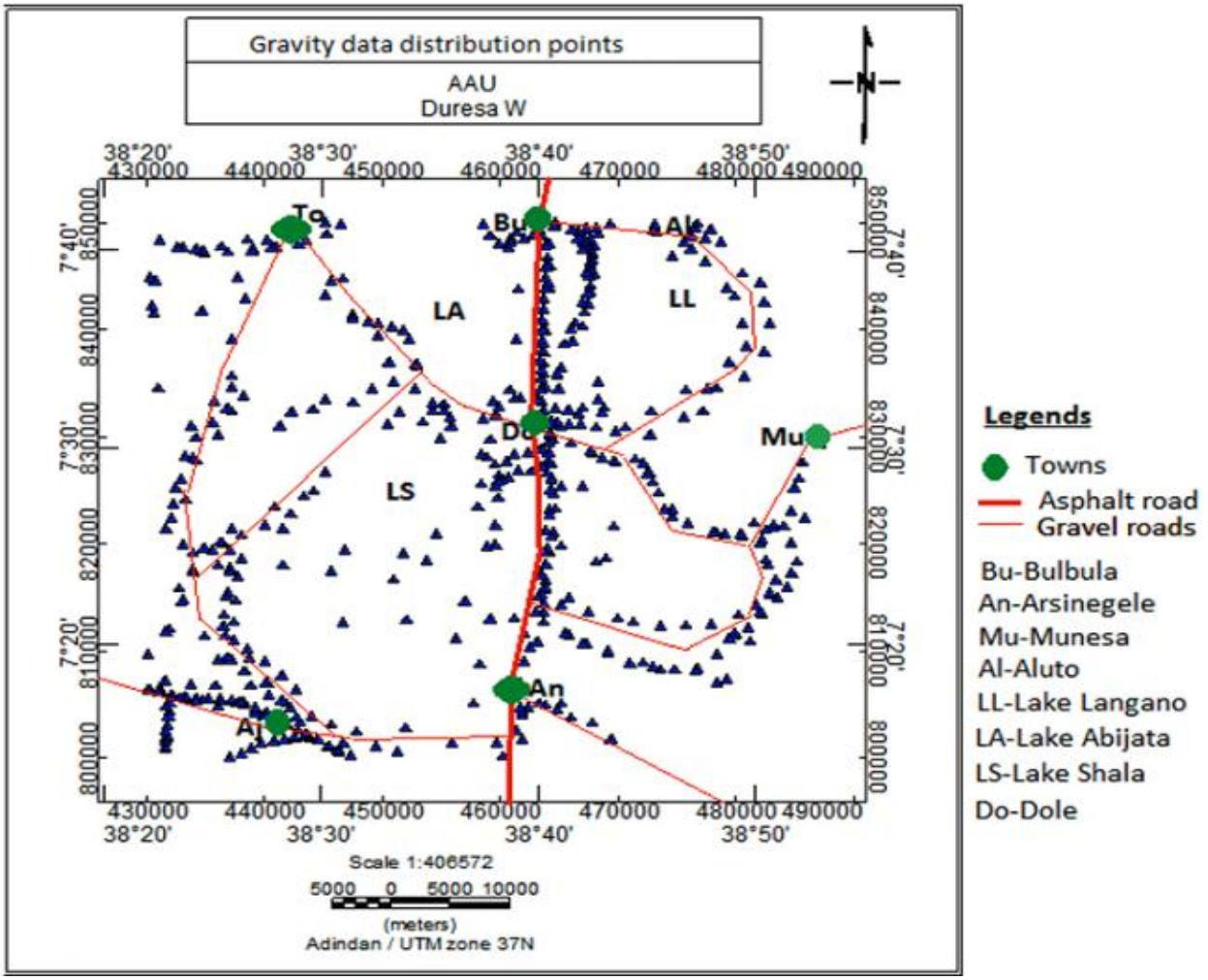

Figure 4- 1 Gravity data distribution of the study area

As can be seen from (Fig.4.1) there is good gravity data coverage throughout the study area. The gravity data obtained for this thesis work were collected by individual researchers (Alemu, 1983, 1992) and the Geological Survey of Ethiopia (EGS).

The secondary data acquired and reprocessed from the work of Alemu (1983; 1992), were collected using the Canadian sharp Gravimeter No. 128 (Worden type gravimeter) and the

Lacoste and Romberg, model G Gravimeter with reading precession of 0.1 and 0.05mgal respectively. On the other hand, the secondary gravity data obtained from EGS as cited in their reports were collected using the Lacoste and Romberg Model 304 gravimeter which also has a precision of 0.05mgal. The survey reports of the secondary data indicate that locations (Latitude, Longitude and elevations) of the gravity stations were determined using classical surveying instruments (altimeters, theodolits, and hand held global positioning system (GPS).All the secondary data obtained are randomly distributed throughout the study area.

The theoretical gravity value at each observation station is computed using the Geodetic Reference System 1967 (GRS67) gravity formula.

4.2 Gravity data processing

4.2.1 Gravity data reduction

All the secondary gravity data have been reprocessed by applying all the standard gravity corrections (drift correction, free air correction, simple and complete Bouguer correction and terrain correction) using average crustal density of 2.67g/cm3. The end results of the survey data the complete Bouguer anomaly values of all the stations considered in the study area have been determined as part of the processing sequence using the Geosoft OasisMontaj (version 7.0) gravity and magnetic data processing and mapping software.

4.2.2 Gravity data gridding and contouring

The final reduced gravity data was compiled in spread sheet excel format with different file extension for the respective software and imported in to Geosoft Oasis Montaj (Version 7.0) for further processing. All the reduced gravity values were gridded using the minimum curvature gridding option of the Geosoft Oasis Montaj software. Following the gridding techniques employed the complete Bouguer anomaly map (Fig. 5.1) were produced.

4.2.3 Regional – residual gravity anomaly separation and data enhancement

The complete Bouguer gravity anomaly represents the total effect of gravity variations caused by deep seated geologic sources that give rise to regional (long wavelength) gravity anomalies and shallow (subsurface) geologic sources that give rise to residual (short wavelength) gravity anomalies. Therefore, it is necessary to separate the complete Bouguer anomaly into its regional and residual components so that we can interpret them independently. This requires estimating

the regional anomaly using an appropriate standard technique to estimate the regional so that the estimated regional component can be subtracted from the complete Bouguer anomaly in order to determine the residual component. There are different techniques (wavelength filtering, upward and downward continuation technique, graphical method, and polynomial trend surfaces filtering technique, etc.) that are applied to separate the complete Bouguer anomaly into its regional and residual components. In this thesis work the 2D FFT Low pass regional filter was used to estimate the regional anomaly by using the Geosoft OasisMontaj software to compile the regional anomaly map (Fig.5.2). The corresponding residual anomaly was computed using the 2DFFT High pass filter to compile the residual anomaly map (Fig.5.3).

4.3 Magnetic data acquisition and distribution

Ground magnetic field was conducted by using the Proton Precision Magnetometer which measures the total magnetic field intensity (TMI). Establishing and positioning of magnetic stations including base stations were done using hand held global positioning system (GPS, GARMIN-12).

Figure 4- 2 Magnetic data acquisition at field.

For this study a single proton precession magnetometer was used in the survey and hence the magnetic data were collected randomly throughout the survey area depending upon the accessibility and field conditions. Accordingly, diurnal corrections and International Geomagnetic Reference Field (IGRF) corrections have been carried out for the collected magnetic data. Generally, In this study a total of about 124 magnetic data has been collected and

this stands as one of the major contributions of this MSc thesis research. In addition about 108secondary magnetic data has obtained from previous MSC research works.

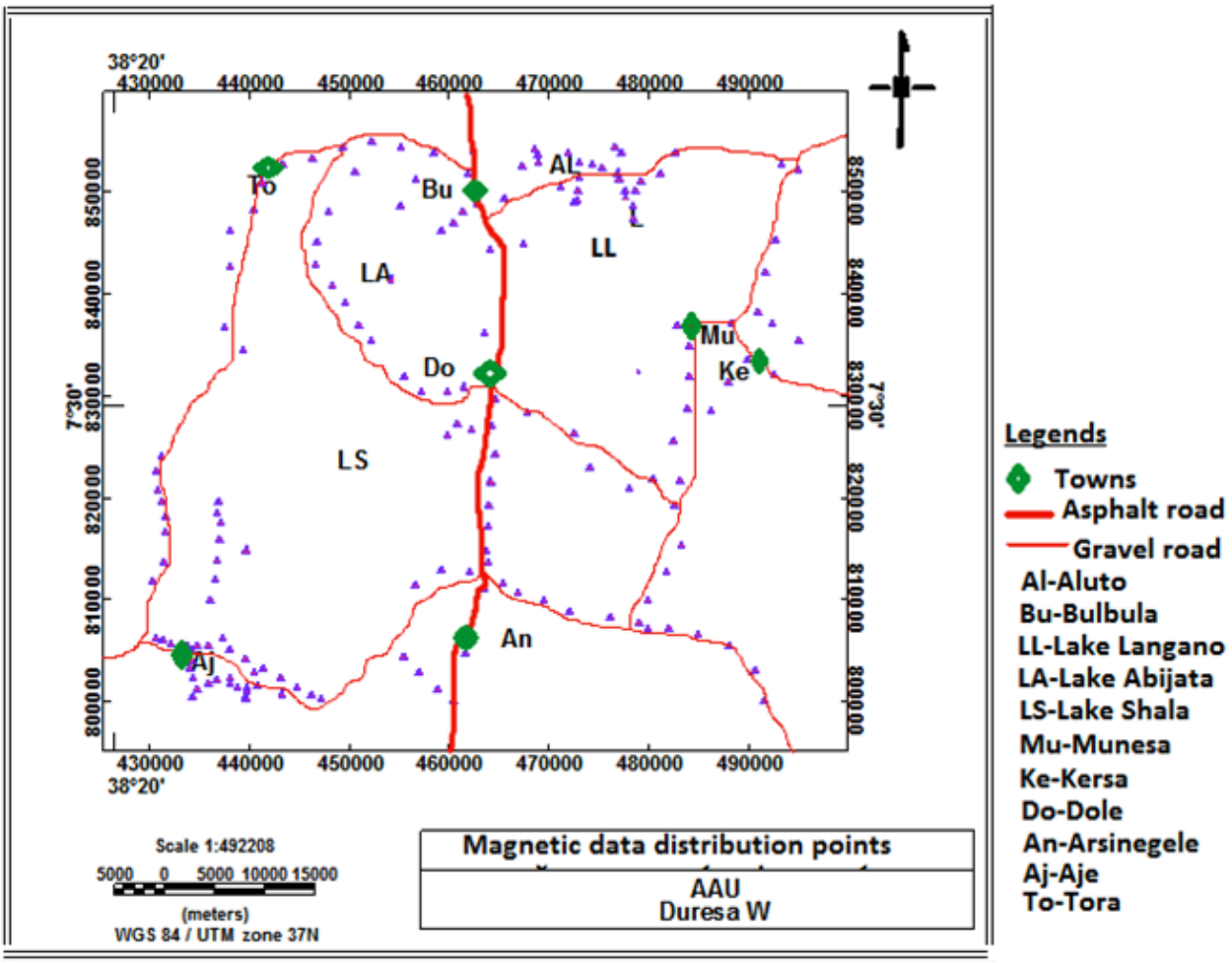

Figure 4- 3 Magnetic data distribution of the study area

Both the new and existing magnetic data were collected along cross-country roads, all weather and seasonal roads at average spacing between 2 to 4Km.

All the primary and secondary data are plotted in (Fig. 4.2). As we can observe from the magnetic data point distribution map, the data density is generally variable throughout the study area being denser around the Aluto volcanic complexes. In contrast to gravity data distribution map (Fig. 4.1), which has a good coverage, the magnetic data distribution map (Fig. 4.2) has a lower coverage.

4.4 Magnetic data processing

4.4.1 Magnetic data reduction

The primary collected magnetic data and the secondary data obtained were corrected for diurnal effects and for the variations caused by dipole field known as IGRF correction (IGRF, 2005) to remove all noises of magnetic variation from the observations other than those arising from subsurface geology it is necessary to make a correction to magnetic raw data.

The total magnetic field anomaly values computed at all the stations considered in the study area are plotted at their locations to compile the total magnetic field anomaly map (Fig. 5.6) of the study area. The total magnetic field anomaly map has been used to compile the regional magnetic anomaly map (Fig. 5.7) and the residual magnetic anomaly map (Fig. 5.8). Furthermore, analytical signal magnetic map (Fig. 5.9), tilt derivative magnetic map (Fig. 5.1) and Euler deconvolution magnetic map (Fig. 5.11) have been compiled for a further enhancement and interpretation in terms of geology of the magnetic data using Geosoft OasisMontaj (Version 6.4.2).

4.4.2 Magnetic data gridding and contouring

Since both gravity and magnetic methods are potential field methods, the gridding and contouring of gravity and magnetic data are more or less the same. Therefore, the total magnetic anomaly data was compiled in spread sheet excel format with different file extensions corresponding to the respective soft wares used. The files with the different file extensions are imported to the Geosoft OasisMontaj (V.7.0) for further processing of the primary data and re-processing of the secondary data. The resulting compiled reduced magnetic data were then gridded using minimum curvature gridding system. Following the gridding techniques the total magnetic anomaly map (Fig. 5.6.) was produced.

4.3.3 Regional-residual magnetic data separation

Like the complete Bouguer gravity anomaly, the total magnetic field anomaly (TMA) map is the total effect of shallow (short wavelength) and regional (long wavelength) anomaly sources. Correspondingly, high pass filtering technique has been applied to the total magnetic field anomaly data in order to determine the residual magnetic anomaly using the Geosoft OasisMontaj software.

CHAPTER FIVE

RESULTS AND INTERPRETATION

5.1 Gravity data results and interpretation

5.1.1 Complete Bouguer gravity anomaly map

Data in the form of Complete Bouguer anomaly (CBA) map can be considered as one of the most important sources of information regarding the subsurface geologic sequence, structure and probable density distributions of a particular survey area. Hence, in order to interpret the subsurface structure contributing for ground water flow within the study area a complete Bouguer anomaly map (Fig.5.1) is produced.

The complete Bouguer anomaly map shows that the Bouguer gravity anomaly field over the study area varies from a relative maximum of -190 mgal to a relative minimum of -225.7 mgal. The northern, north eastern and south eastern parts of the study area are characterized by a minimum value ranging from -220 to -225.7 mgal. These minimum values correspond to the location of Lake Langano, Lake Shala, Lake Abijata and their northern shores which are covered by thick low density alluvium and lacustrine sediments. The relatively minimum values observed around the Bulbula town and the western part of Aluto caldera are caused by thick and low density recent alluvium and lacustrine sediments as observed on the surface geologic map (Fig.2.2) of the study area. Whereas, the north eastern and western parts of the study area show maximum values ranging from -190 to -178 mgal. The locations where the relatively maximum values occur correspond to the locations of the Aluto and Shala volcanic center which is covered by high density volcanic products such as basalts, rhyolite, trachyte and obsidian flows etc. Correspondingly, the high gravity anomaly in the eastern part labelled MU, corresponds to the Munesa ridges which is covered by high density rhyolite intrusions and extrusions exposed on the surface as observed on the surface geologic map (Fig.2.2) of the study area and confirmed by field observations during the magnetic survey.

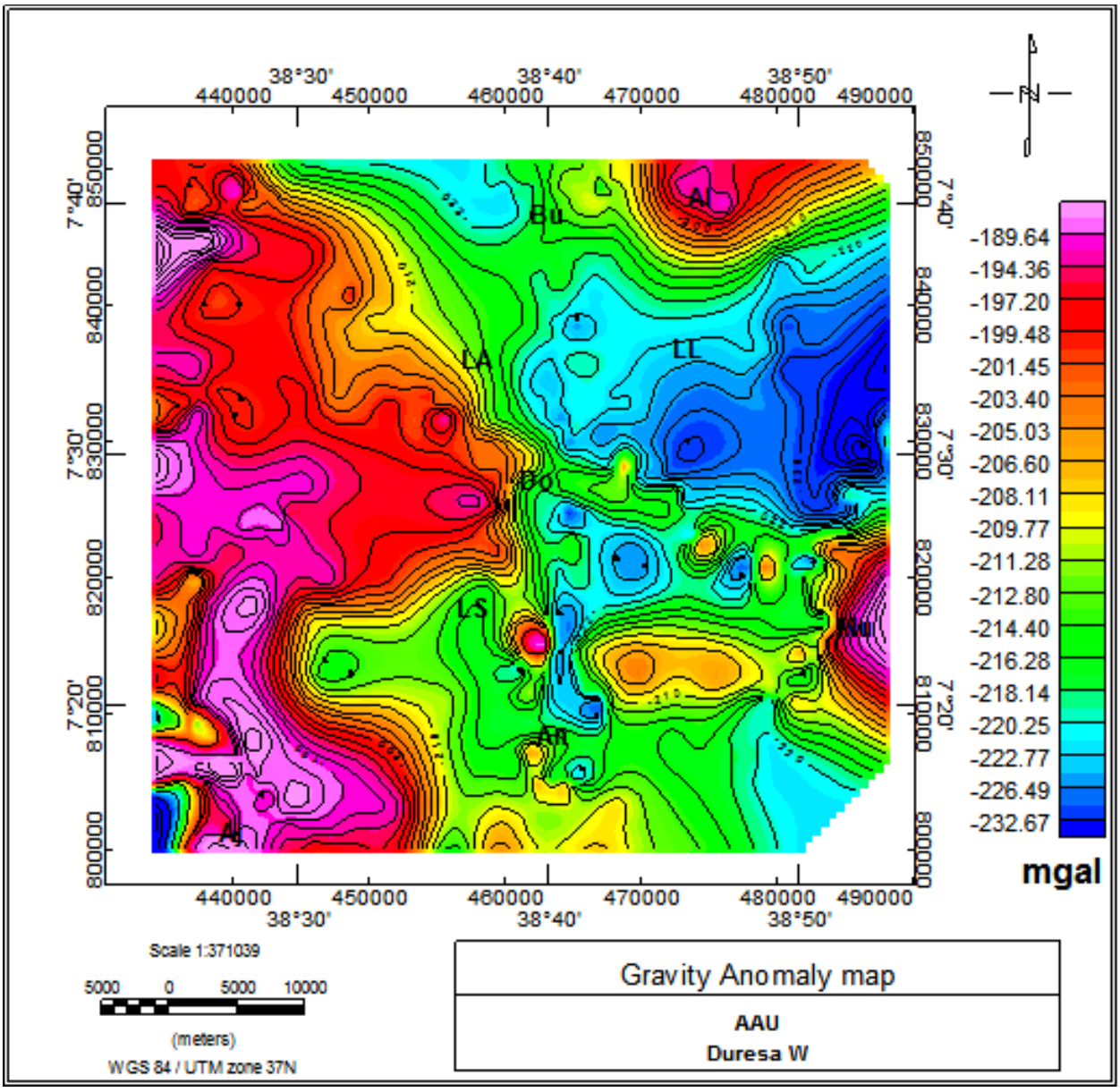

Figure 5.1 Complete Bouguer gravity anomaly map of the study area

The patches of positive anomalies observed on the eastern part can be thought to be caused by segments of the Abadir ridge which is composed of high density volcanic products similar to that of the Aluto volcanic center.

5.1.2 Regional gravity anomaly map

The complete Bouguer anomaly (CBA) is the sum of the effects of features of long wave length, deep seated (regional anomaly) and the near surface, short wave length (residual anomaly)

components. Separation of regional and residual anomaly components is important to see the effects of deep seated and shallow depth sources contributing to the complete Bouguer anomaly. Despite the availability of various methods of separation, a low pass filtering was used in the present work to approximate the regional anomaly using Geosoft OasisMontaj (V.7.0).

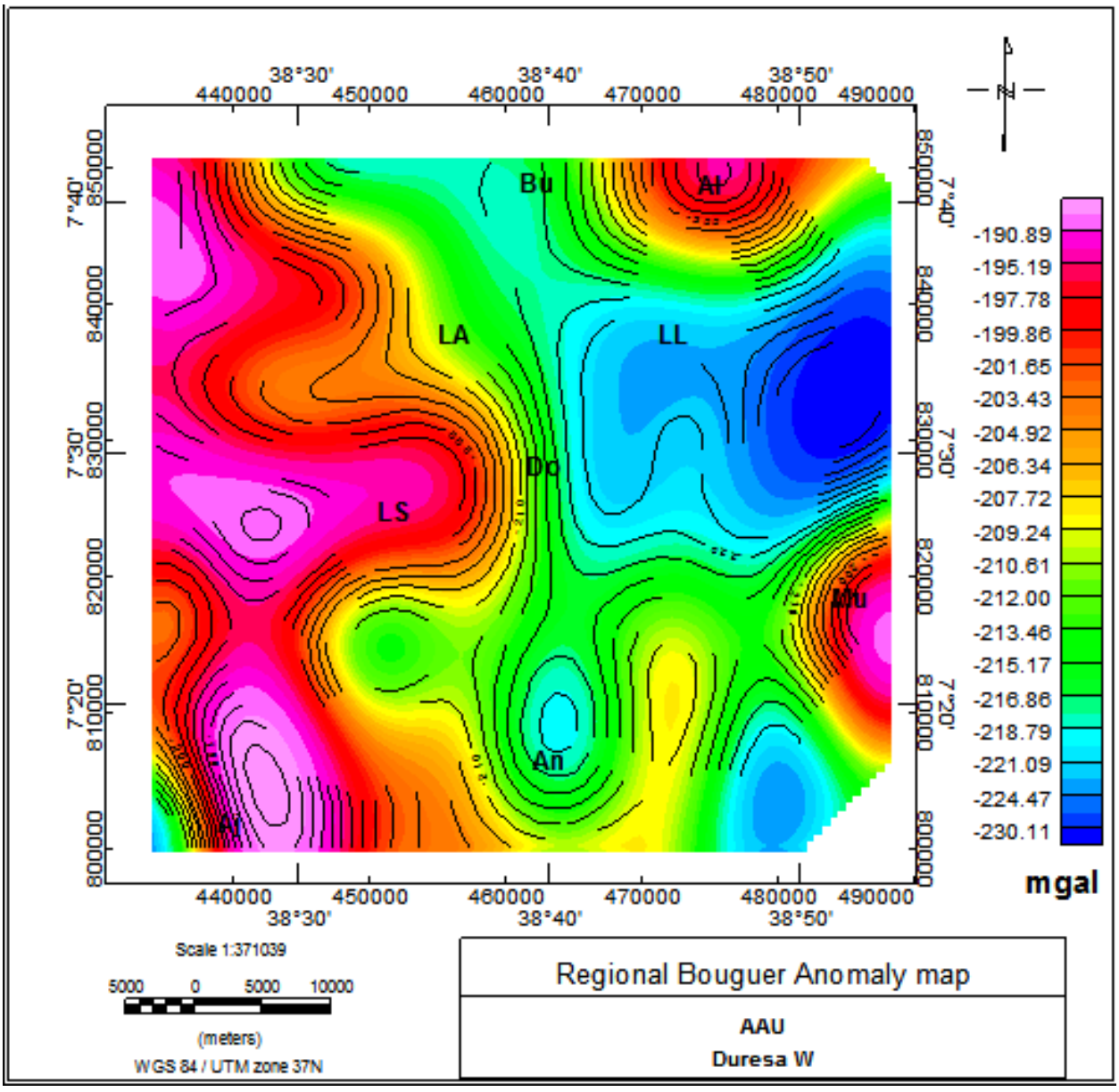

Figure 5.2 Regional Bouguer gravity anomaly map of the study area

The low pass filtered regional anomaly map (Fig. 5.2) of the study area reveals lineated anomalies identified in terms of their location, orientation and relative intensity values. These include:

(1) A zone of positive anomaly engulfing the western part and oriented in approximately NW – SE direction. This anomaly zone is thought to be caused by relatively deep seated high density intrusive bodies beneath the locations of the Aluto volcanic complex and the Shala volcanic center. (2) Relatively negative anomaly zones with values ranging from -225.7 to -219.6 mgal lie south east, east of the positive anomaly zone. These negative anomaly zones can be thought to be the partial effect of the low density volcanic materials composing the eastern plateau.

5.1.3. Residual anomaly map

A high-pass filter is used to obtain the residual anomaly. The residual anomaly map (Fig. 5.3) is compiled after the deduction of the low pass filtered regional anomaly data from the complete Bouguer anomaly data using the Geosoft OasisMontaj Software (V 7.0).

The map is dominated by a number of positive and negative short wave length anomalies occurring as patches of circular and at times elliptical features aligned in E-W, N-S and NW-SE directions. The major positive peaks and the intermediate highs observed over the study area coincide with the localities of the Aluto volcano, Shala caldera and the Munesa ridge. These positive anomalies are associated with relativily high density volcanic rock units as compared to the sedimentary rock units observed on the geologic map (Fig.2.2) of the study area. Particularly, the positive anomaly surrounding Lake Shala can be considered to be caused by ignimbrite, basalt flow cones, and fissural basalt (Fig.2.2). The major negative peaks and the intermediates lows could be attributed to the sediments of the rift floor having varying thickness.

which mainly consist of ignimbrite, fissural basalt, basalt flow, rhyolite and trachyte as

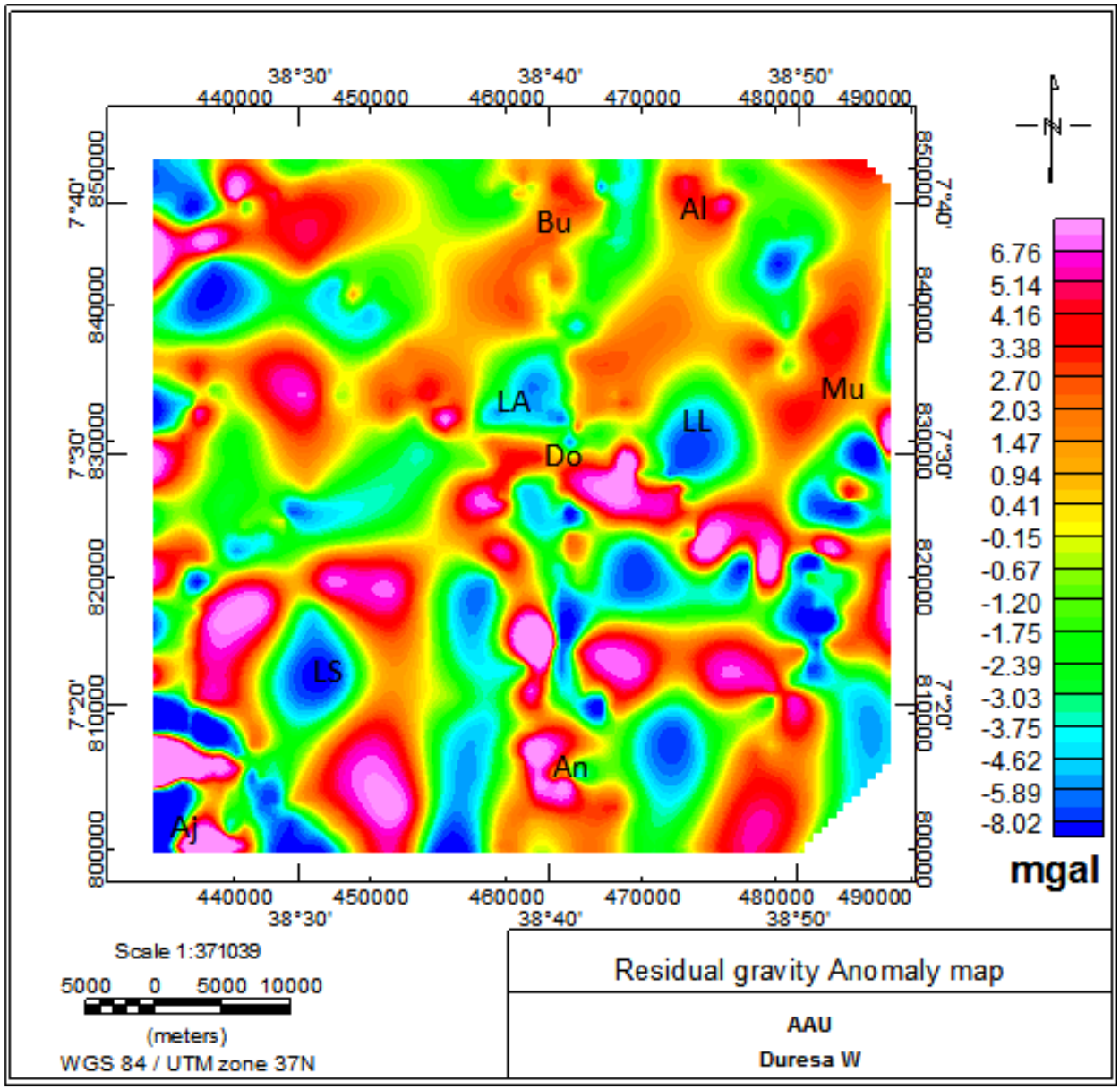

Figure 5.3 Residual Bouguer gravity anomaly map of the study area

5.1.4. Enhancement of the gravity data

5.1.4.1. Horizontal gradient

The horizontal gradient method was used extensively to locate the boundaries of regions of contrasting density from gravity data. The method is based on the premise that the horizontal gradient of the gravity anomaly, which is caused by a planar body, tends to overlie the edges of

the body if the edges are vertical and well separated from each other (Cordell 1979, Cordell and Grauch 1985). Horizontal gradient usually produces exact location of faults.

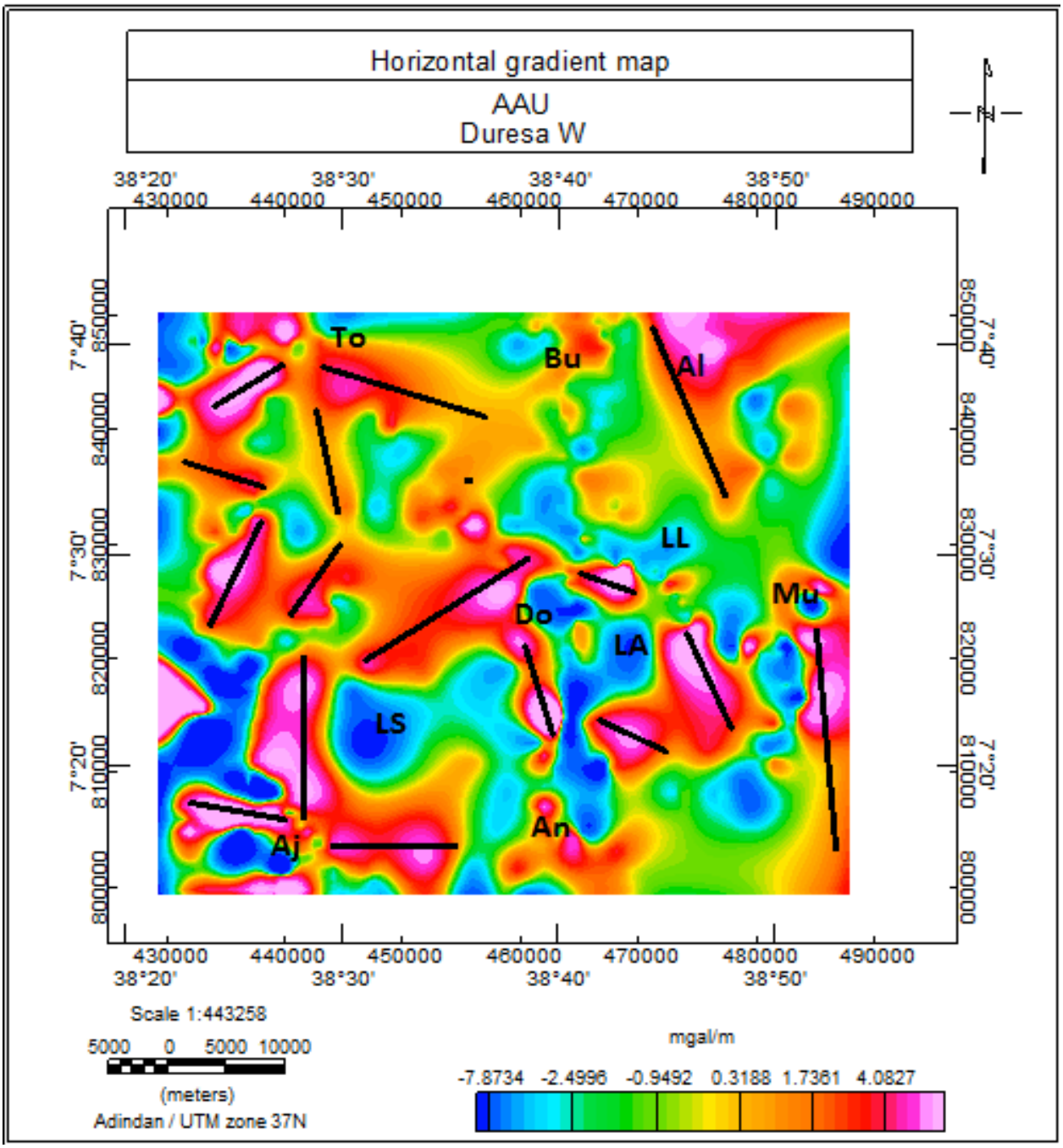

Figure 5- 4 Horizontal gradient gravity anomaly map of the study area

The greatest advantage of the horizontal gradient method is that it is least susceptible to noise in the data because it requires the calculation of only two first-order, horizontal derivatives of the field (Phillips1998). The HG method is robust in delineating both shallow and deep sources.

The horizontal gradient filter can be computed by (Phillips 1998).

$$G(x,y) = \sqrt{(\frac{\partial G}{\partial x})^2 + (\frac{\partial G}{\partial y})^2}$$

Where $\partial G / \partial x$ and $\partial G / \partial y$ are the derivatives of the gravity field in the x and y directions respectively.

The horizontal gradient gravity map (Fig.5.4.) of the survey is compiled from the gridded residual gravity anomaly data. The Locations of the maximum horizontal gradients are shown with black lines superposed along their orientation (Fig .5.4.). These horizontal gradients are anticipated to indicate locations where linear structures (faults, fractures) are occurring in the study area. The orientations of the horizontal gradients are taught to indicate orientation of weak zones that favor the flow direction of groundwater at shallow depths.

The map reveals lineated maximum horizontal gradients which are dominantly oriented in the SE-NW direction in the north western part of the study area. The central part of the study area is dominated by high gradients which are oriented in different directions (do not have the same orientation).

The south western part of the study area is dominated by E-W oriented maximum horizontal gradients. The high horizontal magnitude plots outline lateral mass heterogeneities which are thought to be the expressions of lithological and structural boundaries.

The high gradient magnitudes plots trace linear features trending N-S, The linear features are attributed to faults and fractures, and their continuities are observed in the study area. Moreover the N-S trending linear features (faults and fractures) revealed by the horizontal gradient map can be considered to be the major geologic structures that favor the flow of groundwater within Lake Langano to Lake Abijita and Shala. In line with this there are no east west structures therefore there is no ground water flow from the three lakes to the Munesa ridge.

5.1.4.2. Euler deconvolution gravity map

The Euler Deconvolution is used to estimate the depth and location of gravity source anomalies. The computerized method was developed by Thompson (1982) and is applied for real magnetic data along profiles. Reid *et al.* (1990) followed up a suggestion in Thompson's paper and further developed the method such that it operates for magnetic grid data. Several authors have applied Euler Deconvolution to gravity data, *e.g.*, Corner and Wilsher (1989), Klingele *et al.* (1991), Marson and Klingele (1993), Fairhead *et al.* (1994), and Huang *et al.* (1995). The Euler Deconvolution equation in 3D is given by Reid *et al.* (1990)

$$(x-x_0)\frac{\partial g}{\partial x}+(y-y_0)\frac{\partial g}{\partial y}+(z-z_0)\frac{\partial g}{dz}=n(\beta-g) \tag{5.2}$$

Equation (4) can be rewritten as

$$x\frac{\partial g}{\partial x}+y\frac{\partial g}{\partial y}+z\frac{\partial g}{dz}+ng=x_0\frac{\partial g}{\partial x}+y_0\frac{\partial g}{\partial y}+z_0\frac{\partial g}{dz}n\beta \tag{5.3}$$

where (x_0, y_0, z_0) is the position of a source whose gravity anomaly is detected at (x, y, z), β is the regional value of the gravity, and n is the structural index (SI), which can be defined as the rate of attenuation of the anomaly with distance. The SI must be chosen using prior knowledge of the source geometry. For example, SI = 2 for a sphere, SI = 1 for a horizontal cylinder, SI = 0 for a fault, and SI = –1 for a contact (FitzGerald *et al.* 2004).

The Euler deconvolution gravity map (Fig. 5.5) of the study area is compiled by applying a standard 3D Euler deconvolution filter using the Geosoft OasisMontaj software. The Euler deconvolution gravity map (Fig. 5.5) shows that high clustering of the depth solutions for SI=0.5 are values associated with linear structures at depth levels ranging from less than1km to greater than 3.5km whose locations are plotted on the map with the light red circle, yellow triangle, green octagon, red box, "+" and "x" with different symbols and colors. The map (Fig.5.5) shows linear structures:

-At depths less than 1km are indicated by light red circles. The location of these linear structures is dominantly concentrated at about western, Southeastern and central part of the study area.

- At depths 1-1.5km are indicated by Yellow triangles. The location of these linear structures is dominantly concentrated at about western, central and eastern part of the study area.

-At depths 1.5-2km are indicated by green octagons. The location of these linear structures is dominantly concentrated at about western, eastern and central part of the study area.

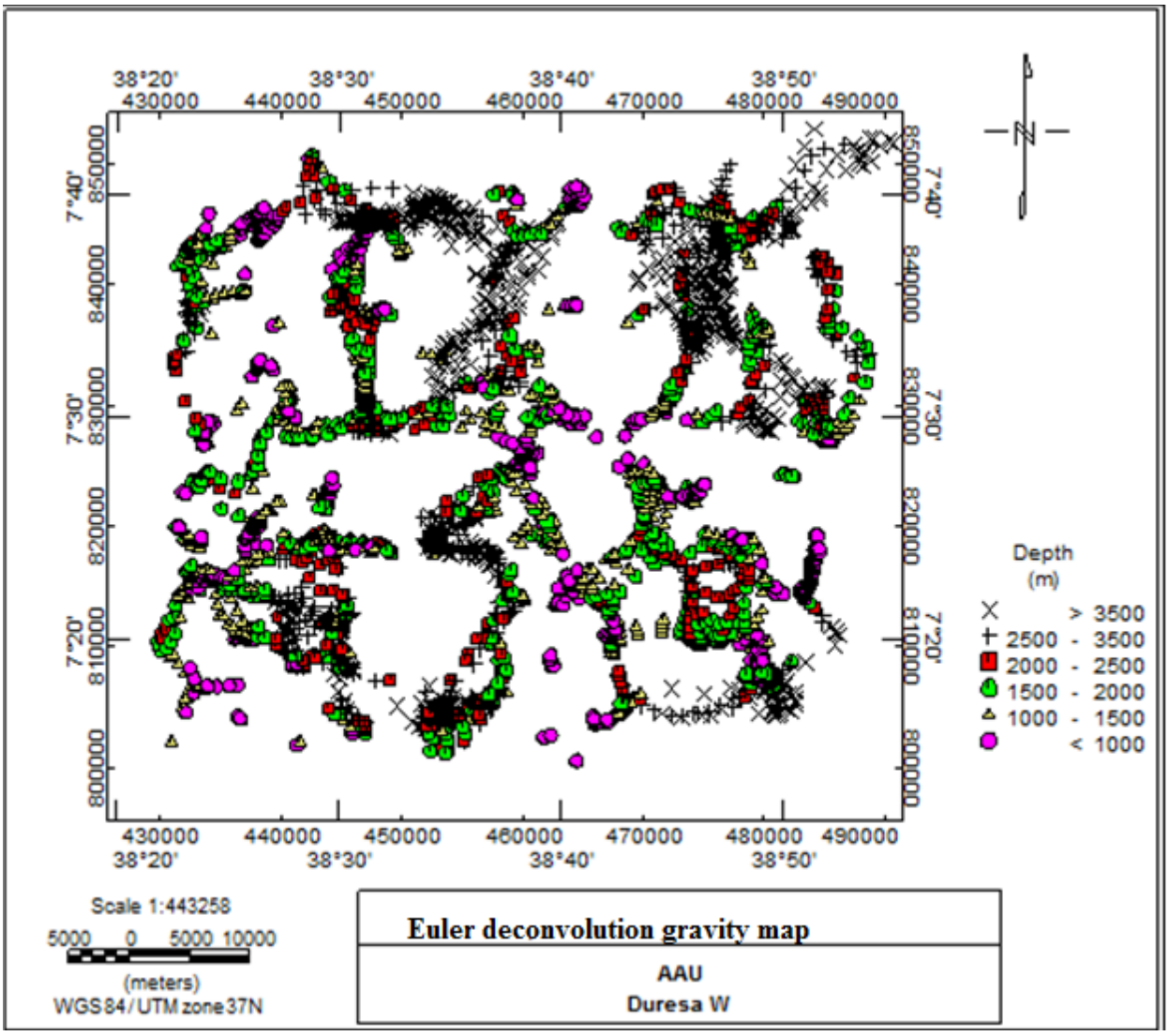

Figure 5- 5 Euler Deconvolution gravity map for SI= 0.5 of the study area

-At depths 2-2.5km are indicated by red box. The location of these linear structures is dominantly concentrated at about western of Lake Shala, Southern of Aluto caldera Southeastern part of the study area.

-At depths 2.5-3.5km are indicated by "+" symbol. The location of these linear structures is dominantly concentrated around Aluto volcanic center, Shala caldera and north western part of the study area.

-At depths greater than 3.5km are indicated by "x" symbols. The location of these linear structures is dominantly concentrated at about Northeastern, Southeastern, central and southwestern part of the study area.

These include a blue circle indicating gravity sources with depth less than 0.5km. The yellow triangle indicates gravity sources that range from 0.5 to 1.5Km depth. The green octagon represents sources that range from 1.5 to 2.5Km depth. The red inverted triangle represents sources that range from 2.5 to 3.5Km depth and the black box represents sources that greater than 3.5km From this we can understand the Aluto and O'a volcanic centers shows shallow volcanic intrusion products and the Munesa shows shallow, intermediate and deep seated faults.

5.2. Magnetic data results and interpretation

The aim of magnetic surveying is to identify and characterize the subsurface structures contribute to ground water flow that is associated with anomalous regions. As a result various magnetic anomaly maps that are assumed to be relevant for this thesis work were produced by following the appropriate reduction procedures has been applied to all the magnetic data using Geosoft OasisMontaj (V. 7.0) software for a further interpretation.

5.2.1. Total magnetic field anomaly map

The magnetic anomaly map (Fig. 5.6) compiled for the study area shows anomaly values ranging from -623 nT to 3 nT. The map shows high to very high anomaly varange -224 to 3nT over Aluto volcanic center, O'a (Shala) volcanic complex, Munesa fault, east of Lake Langano and West of Lake Shala. These high to very high total magnetic anomalies are attributed to either high magnetic susceptibility of magmatic intrusion below the volcanic center.

The map shows low to medium total magnetic anomaly range -412 to -266nT in the central and north western part of the study area. The Shala caldera is characterized by N-S elongated intermediate magnetic anomaly on its western part and it shows low anomaly on its eastern part. The Lakes region occupied by Lake Abiata, Langano, Shala and other parts of the study area are

characterized by low to very low magnetic anomalies, which may be attributed to the thick accumulation of sedimentary rock units (Fig.2.2) bearing low susceptibility values. Geological map (Fig.2.2) and field observations show that the northern shore of Lake Abijata and central part of the study areas are entirely covered by sediments though the thickness of the sediment may vary from place to place. As mentioned earlier these low to very low anomalies are possibly due to the low magnetically susceptible sediments which are possibly derived from the neighboring volcanic materials that have high magnetic contents.

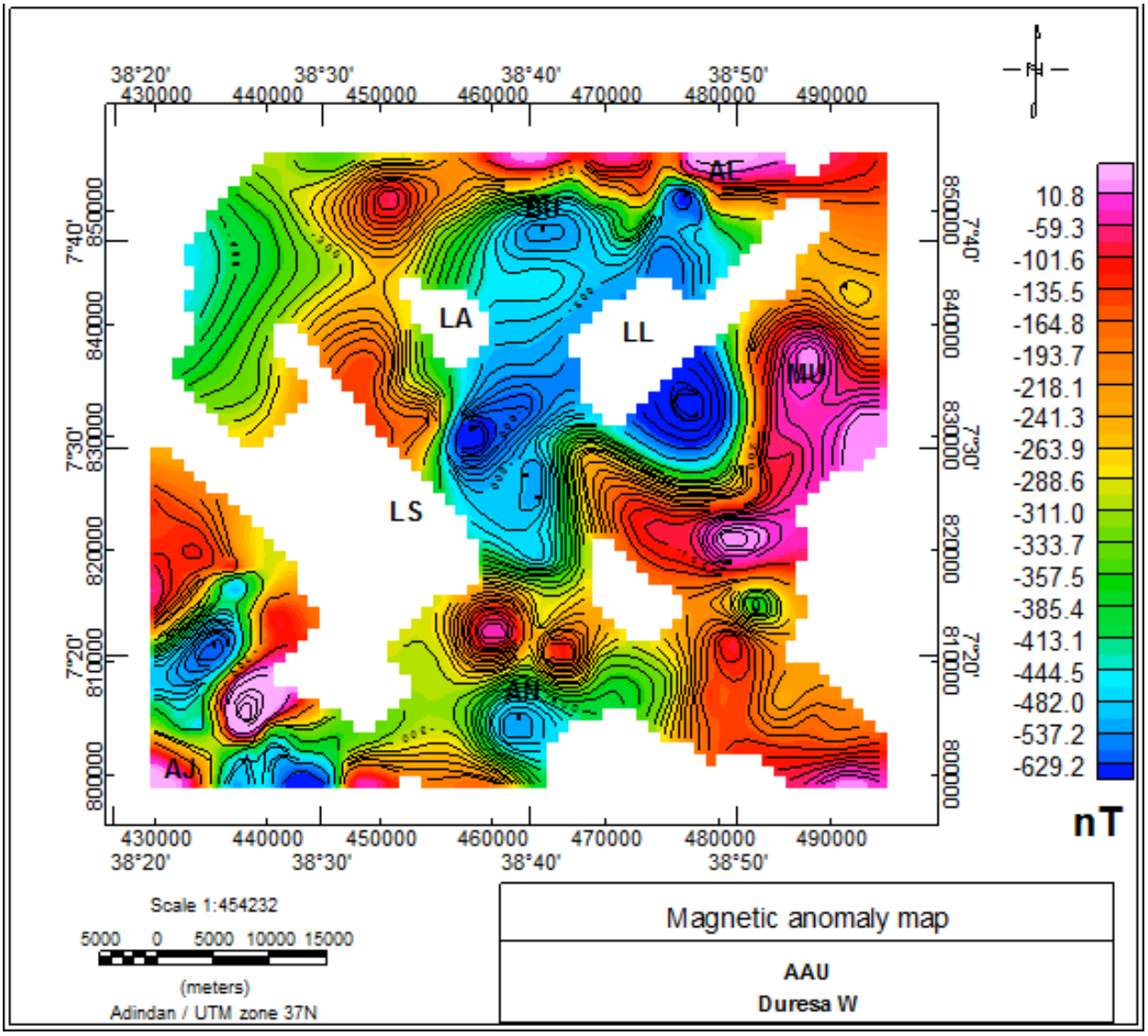

Figure 5.6 Total magnetic anomaly map of the study area

5.2.2. Regional magnetic field anomaly map

The regional magnetic anomaly map of the study area was generated by applying a low pass filtering technique using the Oasis GeosoftMontaj Software (V7.0).

The regional magnetic anomaly map (Fig. 5.7) reveals four distinct zones with alternating bands of negative and positive magnetic anomalies over the study area from east to west.

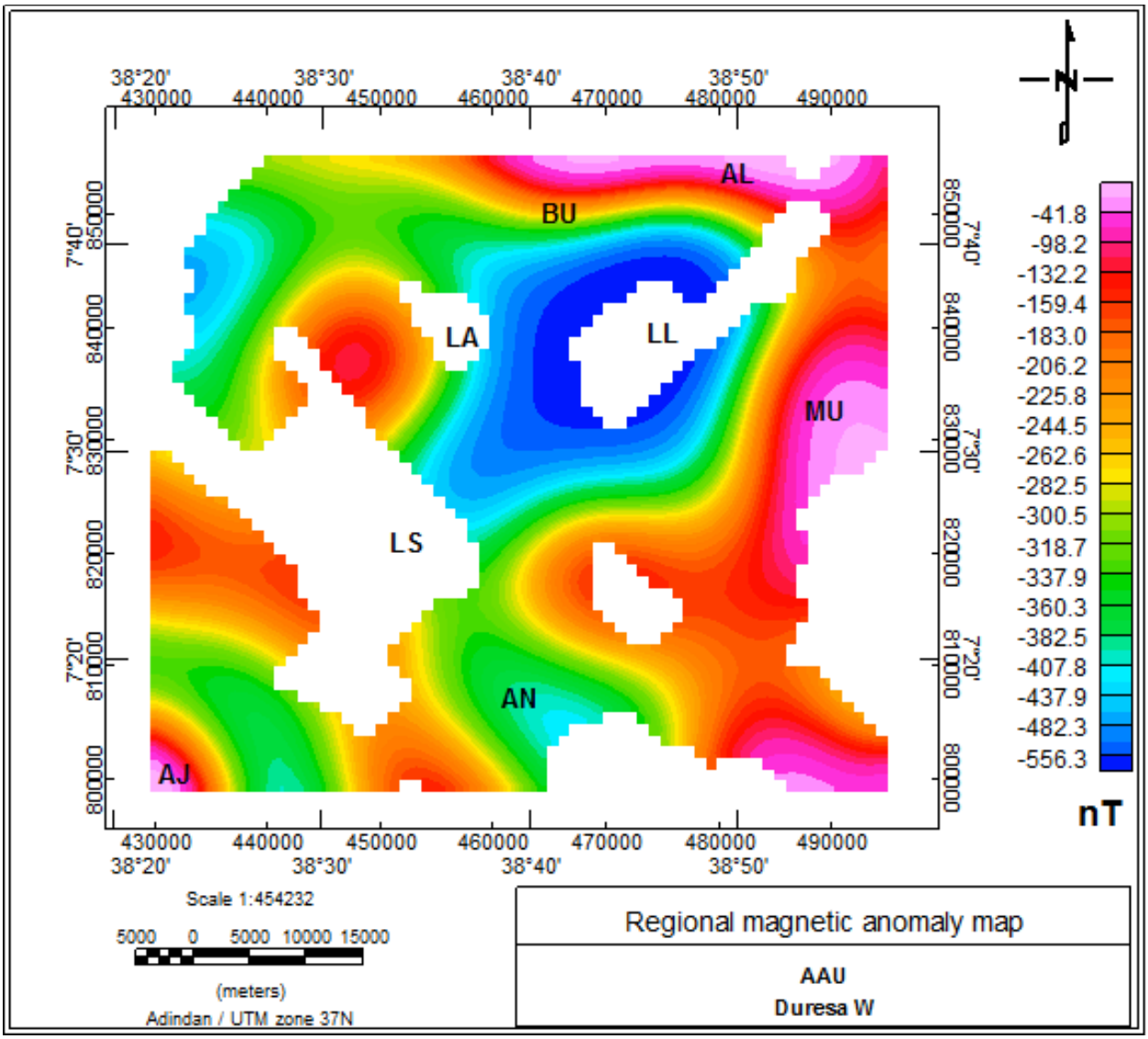

Figure 5.7 Regional magnetic anomaly map of the study area

The first zone which coincides with the locations of Aluto volcanic center, O'a volcanic complex, Abadir ridge and Munesa ridge is characterized by a relatively high to very high (-207 to -36 nT) magnetic anomalies with the highest peak occurring at the western part of the Aluto and southern part of O'a volcanic center. The second zone which coincides with the location of

Lake Langano, Abijata, Shala and their flanking areas are associated with a broad negative magnetic anomaly The third zone which coincides with the location of Lakes Abiata, Langano, Shala and the flanking areas is characterized by a broad negative anomaly varying from -417nT to -571nT.

The high magnetic anomaly zones observed over the study area are associated with the low susceptibility (heat treated volcanic materials) related to the associated volcanic centers. In particular the magnetic highs over Aluto and O'a volcanic centers are correlated with the low magnetic susceptibility geologic bodies beneath the volcanic centers or calderas. Moreover, the high magnetic anomalies over the locations of the Goljota and surrounding areas and Munesa faults are due to the low magnetic susceptibility rocks exposed in the area (Fig. 2.2).

The first and third low magnetic anomaly zones coinciding with the locations of Lake Langano, Abijata, Shala and their flanking areas is attributed to the thick accumulation of high magnetic susceptibility sediments that are derived from the surrounding volcanic units.

The northern and central part of the study area is characterized by low to very low regional magnetic anomalies. As explained earlier the regional gravity anomaly shows N-S an oriented magmatic intrusion beneath Shala caldera which is invisible in the regional magnetic anomaly. This is due to the inherent problem of magnetic anomaly interpretation at low latitude zones where a N-S oriented magmatic intrusion/dike injection is not clearly identifiable.

5.2.3. Residual magnetic field anomaly map

The residual magnetic anomaly (TMA) map (Fig.5.8) of the study area was generated after removed the regional magnetic field using high pass filter analysis using Geosoft OasisMontaj Software (V.7). It represents volcanic centers and structural features of intermediate and shallow depths with a general NNE-SSE, NE-SE and E-W trending structures. The prominent geological features observed in the residual magnetic anomaly map are generally preserved in the total and regional magnetic anomaly maps (Figs.5.8 and 5.9.) However, the residual magnetic anomaly map defines areas like O'a volcanic complex, Aluto volcanic center and Munesa ridge with very high magnetic anomalies than in the total and regional magnetic anomaly maps. This indicates that the main sources of these magnetically anomalous zones found within or close to the WFB

are probably found at shallow depths. Further, areas like, west of Aluto plateou associated with intermediate magnetic anomalies.

Field observations indicate that the observed residual magnetic anomalies are also governed by the distribution of geologic materials and geologic structural features. This implies that areas covered by basaltic and scoraceous rocks are associated with positive magnetic anomalies.

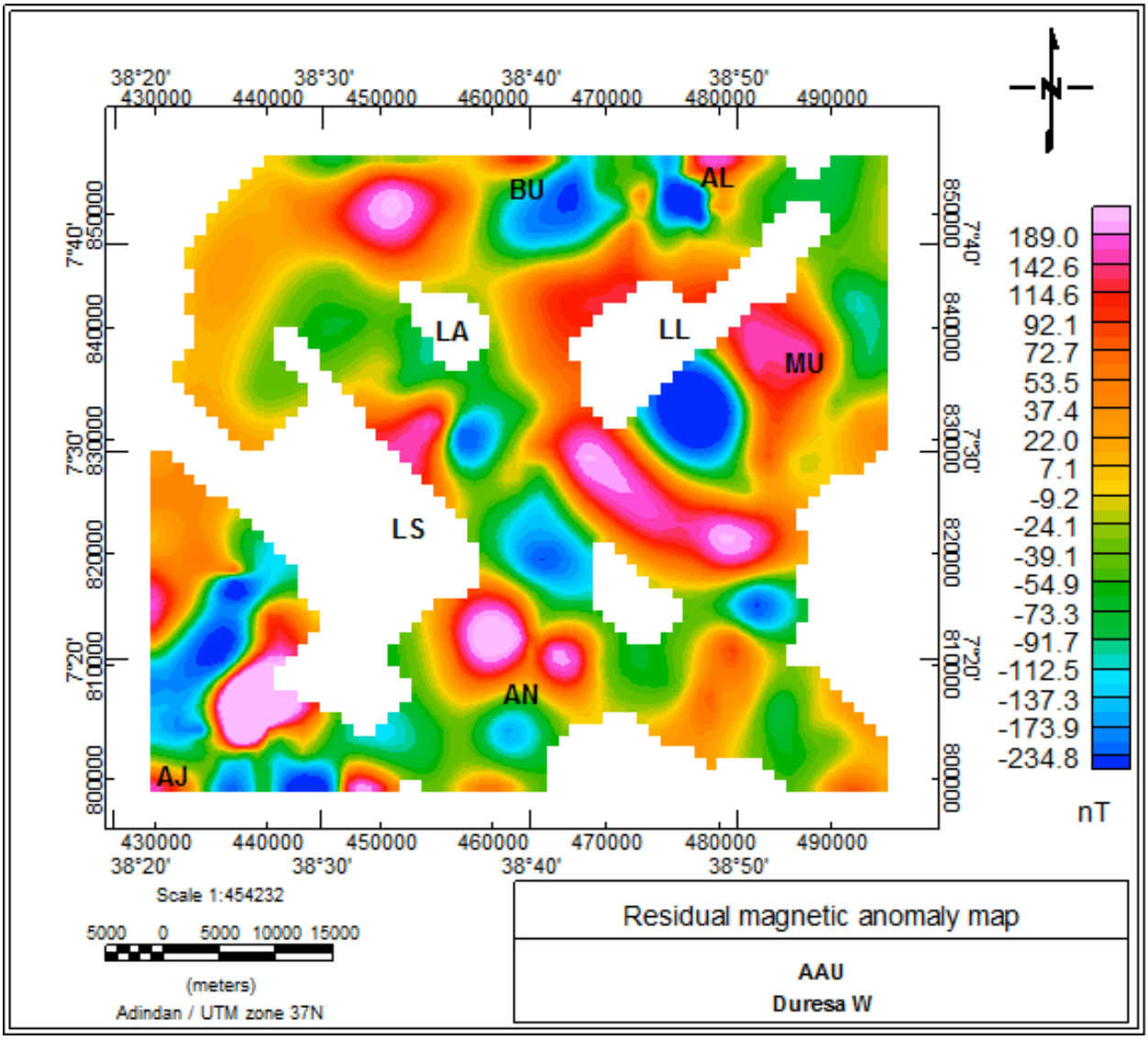

Figure 5.8 Residual magnetic anomaly map of the study area

This is evident in east of Lake Langano is concentrated by basaltic rocks and related scoraceous materials. Since the study area is located at low magnetic latitude (magnetic equatorial region), there exists an inverse relationship between nature of magnetic susceptibility of the geologic

bodies/sources and their associated magnetic anomalies. Therefore, the high to very high magnetic anomalies depicted over the volcanic centers are attributed to low magnetic susceptibility geologic materials beneath these silicic volcanic centers.

In contrary, the negative magnetic anomaly zone which covers most of the Lakes region and associated depressions and part of the highland are attributed to high magnetic susceptibility sediments derived from the neighboring volcanic rocks.

5.2.4. Analytical signal magnetic map

According to Dentith and Mudges (2014) the analytical signal map of a magnetic field anomaly data is produced by combining the 3-directional gradients of the magnetic field anomaly at the locations (x, y, z) considered and given by:

$$AS(\mathrm{x},\mathrm{y}) = \left(\sqrt{\left(\frac{\partial \Delta A}{\partial x}\right)^2} + \sqrt{\left(\frac{\partial \Delta B}{\partial y}\right)^2} + \sqrt{\left(\frac{\partial \Delta C}{\partial z}\right)^2}\right) \qquad (5.2)$$

Where: ΔB is the magnetic field anomaly considered.

Generally, the interpretation of magnetic data is difficult at low magnetic latitudes due to the complex nature of magnetic field at the equator/low latitude. However, the magnitude of analytical signal map produces maximum value over magnetic contacts regardless of the direction of magnetization and is always positive.

The analytic signal map (Fig.5.9.) of the study area is obtained from the residual magnetic anomaly data using Geosoft OasisMontaj software. The analytic signal map reveals magnetic anomalies that result from vertical and horizontal variations of the anomaly. As can be revealed from the map, the maximum values of the analytic signal map are generally coincident with the magnetic anomaly peaks observed in the residual magnetic anomaly.

Susceptibility contrasts in the basaltic units result in large gradients in the unit as compared with the surrounding sediments and low magnetic susceptibility rock units like ignimbrite and rhyolite. This is evident in the eastern and south eastern part of the study area where the

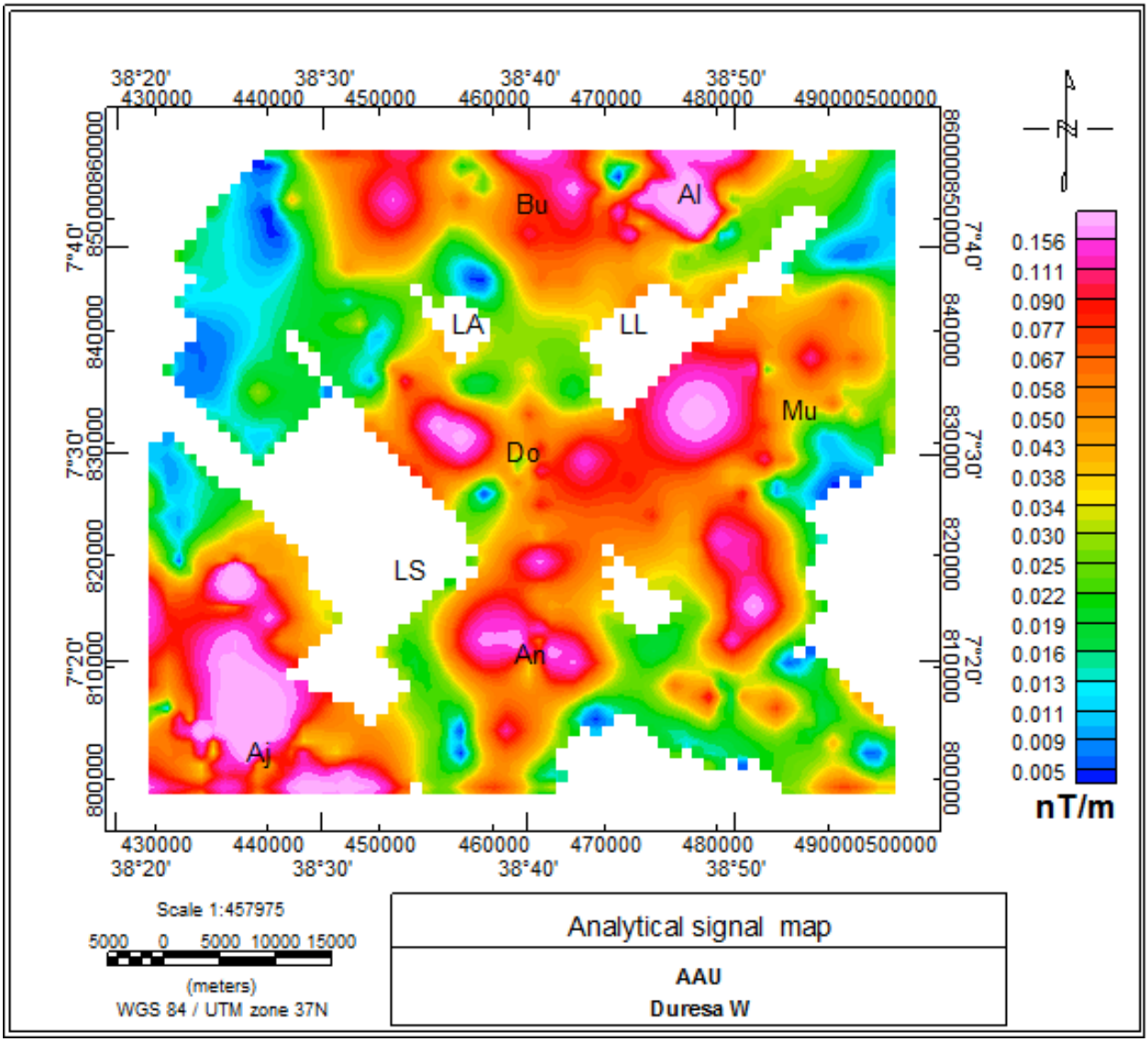

Figure 5.9 Analytical signal magnetic map of the study area

Pleistocene basalt shows a high analytic signal value due to the high susceptibility contrast as compared with the surrounding units. The low magnetic anomalies of the Lake Abiata observed in the residual anomaly map are now characterized by intermediate to high peaks of analytic signal map. This result from the active faults that start at the southern end of Aluto volcanic center, pass between Lake Langano and Lake Abiata. Most of the structures follow the N-S and NNE-SSW trend. In fact, there are also some basaltic units exposed in the NE and northern shores of Lake Langano which appear to enhance the analytic signal values.

5.2.5. Tilt derivative magnetic map

In order to identify the location of contacts/boundaries and faults in the study area tilt derivative filter was applied to the analytical signal map in order to compile a tilt derivative magnetic map (Fig.5.10) of the study area using Geosoft OasisMontaj software (V.7.). The main advantage of tilt derivative map is that it can be used to locate edges and geological boundaries.

The tilt derivative magnetic map (Fig.5.10) shows more detailed structural contacts/boundaries than the analytic signal magnetic map. It shows positive values over magnetic sources, cross through zero at or near the fault/contact locations and negative outside source zones.

Accordingly, the study area is characterized by numerous faults oriented in the N-S, NE-SW and NW-SE directions. These directions are correlated with the general tectonic history of the MER with abundant N-S and NE-SW trending structures. There are also some other fault trends with NW-SE orientation indicated by the tilt derivative map of the study area.

The N-S, NE-SW lineated structures (faults and fractures) observed on the tilt derivative magnetic map appear to be consistent with the N-S, NE-SW lineated structures mapped on the horizontal gradient gravity map (Fig. 5.4) of the study area.

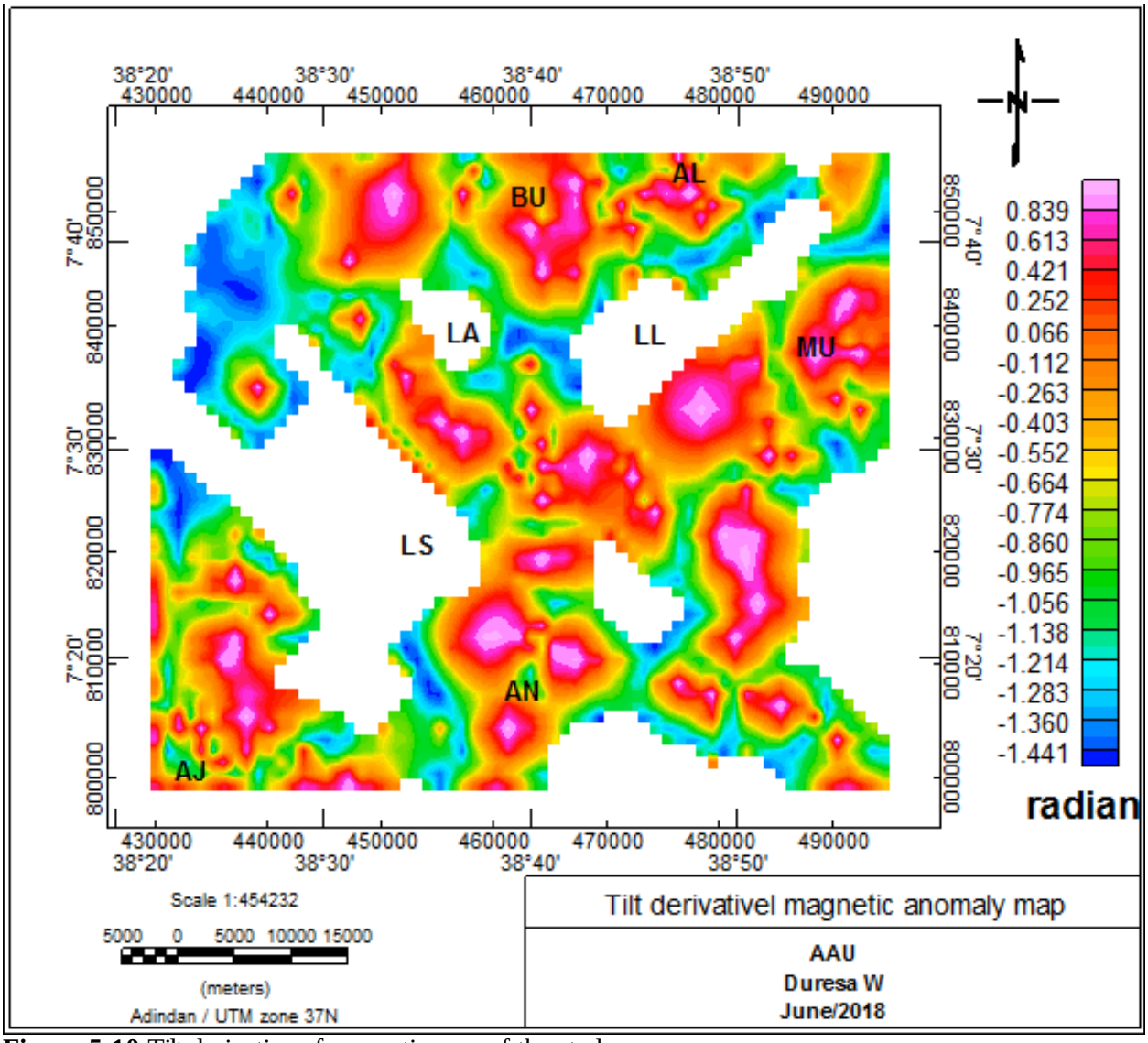

Figure 5.10 Tilt derivative of magnetic map of the study area

Thus, the N-S trending lineated features (faults and fractures) revealed by both the horizontal gradient gravity map and the tilt derivative magnetic map can be considered to be the major geologic structures that favor the flow of ground water within Lake Langano to Lake Abijita and Lake Shala. In line with this both maps appear to show that there are no east west lineated structures that favor the flow of groundwater from the three Lakes towards rift margin of the study area.

Therefore, the direction of groundwater flow in the study area takes place from Lake Langano towards Lake Abijita Lake Shala being controlled by the N-S and NE-SW oriented faults and fractures.

5.2.6. Euler deconvolution magnetic map

Euler deconvolution technique is applied to the total magnetic anomaly in order to estimate the depth and location of the magnetic source. In standard Euler deconvolution process, each model contains solutions of a particular structural type defined by a structural index. From the principle of Euler deconvolution the structural index values 0, 1, 2, 3 represent geological features of contact, sill/dike, vertical pipe/horizontal cylinder and sphere respectively.

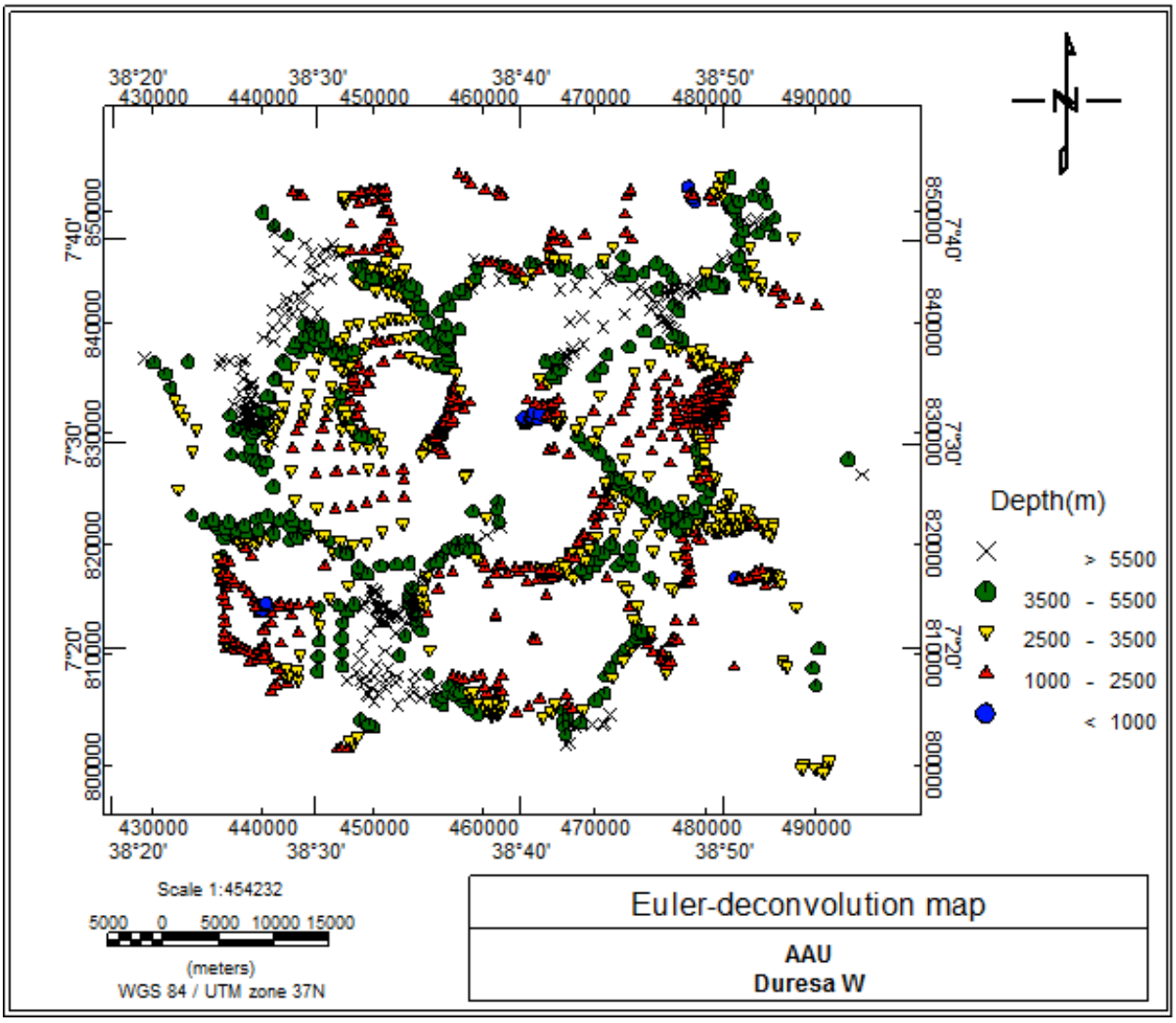

Figure 5.11 Euler deconvolution magnetic map for SI = 0.5 of the study area

The Euler deconvolution map (Fig. 5.11) of the study area is compiled by applying the standard 3D Euler deconvolution filter using the Geosoft OasisMontaj software. The optimal structural

index is selected by a visual inspection of maps which are compiled using various structural indices until the best clustering of solutions is obtained.

Based on this procedure, a structural index of (SI=1) was determined and applied to the total magnetic anomaly map to compile the Euler deconvolution map (Fig. 5.11). The map reveals magnetic sources of different depths marked by different colored symbols plotted on the map. These include the blue circles indicating magnetic sources with depth less than 1Km, The red triangles indicating magnetic sources that range from 1km to 2.5 Km depth. The the yellow inverted triangles represent sources that range from 2.5 to 3.5 Km depth. The green octagon represents sources that range from 3.5km to 5.5km depth. The symbols marked by the symbol "x" represent sources that are greater than 5.5 Km depth.

The distribution of the sources (shallow, intermediate and deep sources) over the study area revealed by the Euler deconvolution magnetic map (Fig. 5.11) appear to be consistent with the distribution of the sources revealed by the Euler deconvolution gravity map (Fig. 5.5).

5.3 Qualitative interpretation of the gravity and magnetic survey results

In the study area, most of the high anomaly responses from the geophysical methods utilized in the present work show a close correlation in delineating the subsurface geologic structural features beneath localized zones. The observed comparatively positive anomalies largely occur at the locations of the volcanic complexes. In contrast, the observed relatively negative geophysical anomaly responses appear to be associated with the areas that lie adjacent or away from the volcanic complexes, particularly close to the shores of Lake Ziway and Lake Langano.

In qualitative terms, the gravity highs (refer to the different gravity anomaly maps under section 5.1) and the magnetic highs (refer to the different magnetic anomaly maps under section, 5.2) considered in the study area are associated with the zones that are characterized by the volcanic centers.

The gravity highs and magnetic highs are exclusively linked with the volcanic centers of Aluto in the North/NE in the Central sections of the study area.

Interpretations of the geophysical responses vary from one method to another, as far as resource exploration, particularly subsurface structure is considered, the geophysical survey tools seeks to

delineate the gravity and magnetic methods are used to delineate the subsurface structures which favor for the formation of ground water.

The gravity and magnetic highs in almost all of the maps generated (depicted under sections 5.1 and 5.2), are associated with the Aluto volcanic complex in the study area.

All the geophysical investigation results leads to the conclusion that the shallow depth subsurface structures identified beneath the study area control the ground water flow from Lake Langano to LakeAnijata and Lake Shala.

5.3.1 2D Gravity modeling

To give a tentative quantitative interpretation regarding the subsurface lithological units of the study area a 2D gravity modeling was constructed along profile P1and profile P2 (Fig 5.13) in the study area.

The gravity models are prepared using the anomaly values extracted from the residual Bouguer gravity anomaly map (Fig. 5.3) also given here below. The Geosoft Oasis Montaj GM-SYS 2D gravity modeling software is used for both models. A priori density model was obtained from the work of Saibi (2012) in the Aluo geothermal system. Accordingly, the first layer consists of Quaternary volcanic products of Aluto volcano (ash flow tuffs, silicic lithic tuff breccias, silicic domes, pumice). The second layer consists of Pleistocene–Holocene lacustrine sediments with an average thickness of 400m. The third layer includes fissural basalt, named the Pliocene Bofa basalt; the unit has a thickness of approximately 800 to 1000 m. The fourth layer is represented by Tertiary ignimbrite (silicic unit) with a thickness of 700 m.

5.4 Qualitative interpretation of the gravity and magnetic survey results

In the study area, most of the high anomaly responses from the gravity and magnetic methods utilized in the present work show a close correlation in delineating the subsurface geologic structural features beneath localized zones. The observed comparatively positive anomalies largely occur at the locations of the volcanic complexes. In contrast, the observed relatively negative geophysical anomaly responses appear to be associated with the areas that lie adjacent or away from the volcanic complexes, particularly close to the shores of Lake Langano, Lake Abijata and Lake Shala.

In qualitative terms, the gravity highs (refer to the different gravity anomaly maps under section 5.1) and the magnetic highs (refer to the different magnetic anomaly maps under section, 5.2) considered in the study area are associated with the zones that are characterized by the volcanic centers.

The gravity highs and magnetic highs are exclusively linked with the volcanic centers of Aluto in the North/NE in the Central sections of the study area.

Interpretations of the geophysical responses vary from one method to another, as far as resource exploration, particularly subsurface structure is considered, the geophysical survey tools seeks to delineate the gravity and magnetic methods are used to delineate the subsurface structures which favor for the formation of ground water.

The gravity and magnetic highs in almost all of the maps generated (depicted under sections 5.1 and 5.2), are associated with the Aluto volcanic complex in the study area.

All the geophysical investigation results leads to the conclusion that the shallow depth subsurface structures identified beneath the study area control the ground water flow from Lake Langano to Lake Abijata and Lake Shala.

5.4.1 2D Gravity modeling along p1 and p2

To give a tentative quantitative interpretation regarding the subsurface lithological units of the study area a 2D gravity modeling was constructed along profile P1and profile P2 (Fig 5.13) in the study area.

The gravity models are prepared using the anomaly values extracted from the residual Bouguer gravity anomaly map (Fig. 5.3) also given here below. The Geosoft Oasis Montaj GM-SYS 2D gravity modeling software is used for both models.

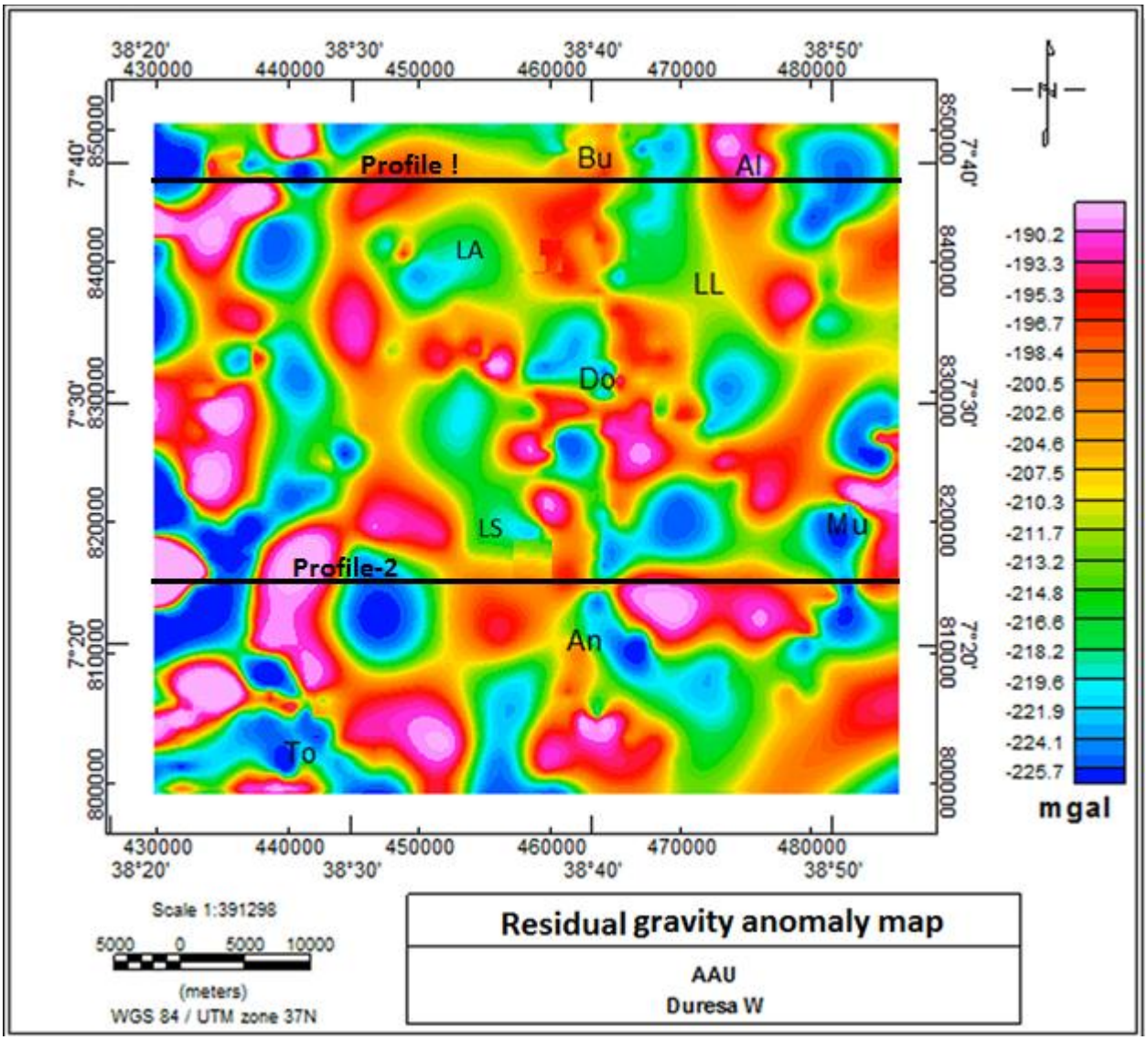

Figure 5.12 Residual gravity anomaly shows profiles for 2D modeling

A priori density model was obtained from the work of Saibi (2012) in the Aluo geothermal system. Accordingly, the first layer consists of Quaternary volcanic products of Aluto volcano (ash flow tuffs, silicic lithic tuff breccias, silicic domes, pumice). The second layer consists of Pleistocene–Holocene lacustrine sediments with an average thickness of 400m. The third layer includes fissural basalt, named the Pliocene Bofa basalt; the unit has a thickness of approximately 800 to 1000 m. The fourth layer is represented by Tertiary ignimbrite (silicic unit) with a thickness of 700 m.

5.4.1.12D Gravity model along profile P1

The 2D gravity model (Fig. 5.13) is constructed along profile P-1 runs in east - west direction which is aimed to show variation in density and lithological units across the Bulbula-Arsinegele rift corridor.

The 2D gravity model (Fig. 5.13) constructed along profile P-1consists of four layers based on the depth / lithology and density constraints considered for the initial model. A further adjustment of these parameters resulted in a fit between the observed and calculated gravity values (Fig. 5.13). The error determined for the fit between the observed and calculated gravity values is 0.528 %.

The final gravity model corresponding to the first layer consists of relatively low density near surface volcanic ash products with an average density value of about 1.7 gm/cm^3. The average thickness of this layer varies from 100-200 m. The second Layer has an average density value of 1.9 gm/cm^3 is interpreted as pleistocine – holocine lacustrine Sediment and underlain by Basalt rocks with an average thickness ranging from 450-650m. The third layer shows thick fissural

Basalt at the top of Aluto and thin Basalt deposit in the Aluto caldera. The fourth layer is interpreted as ignimbrite rocks overlain by Basalt rocks with an average thickness ranging from 1400-1850m.

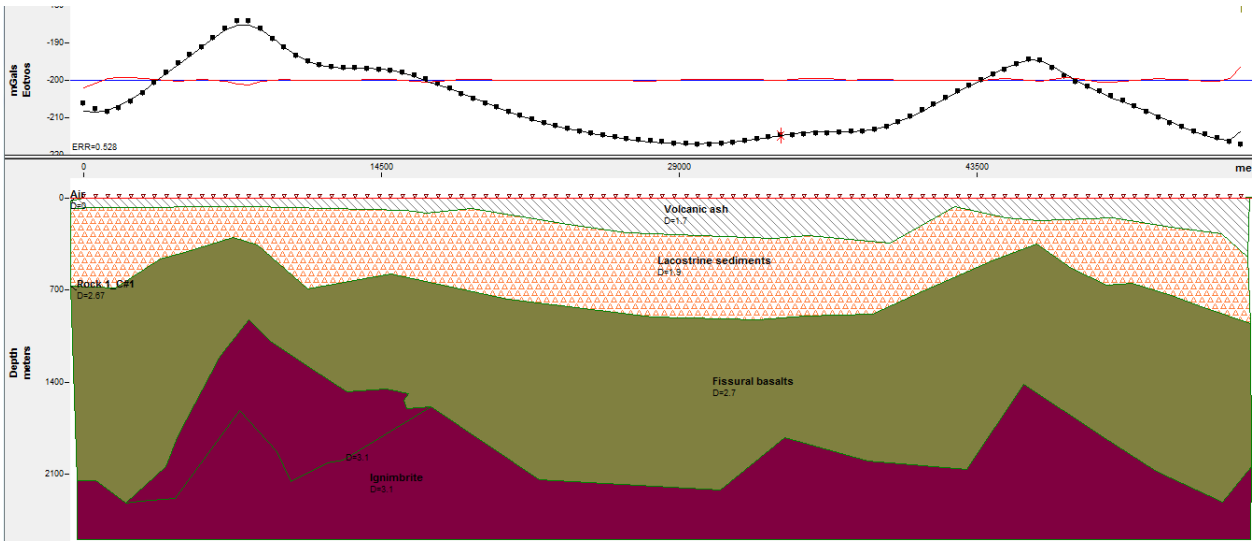

Figure 5.13 2D gravity modeling along profile-1 of the study area

5.4.1.2 2D Gravity model along profile P2

The 2D gravity model (Fig. 5.14) is constructed along profile P-2 runs in a east- west direction which is aimed to show variation in density and lithological units along the Bulbula-Arsinegele rift corridor. The model consists of four layers determined on the basis of the depth / lithology and density constraints considered for a priori model. A further adjustment of the initial parameters resulted in a fit between the observed and calculated gravity values (Fig. 5.14). The error determined for the fit between the observed and calculated gravity values is 0.61%.

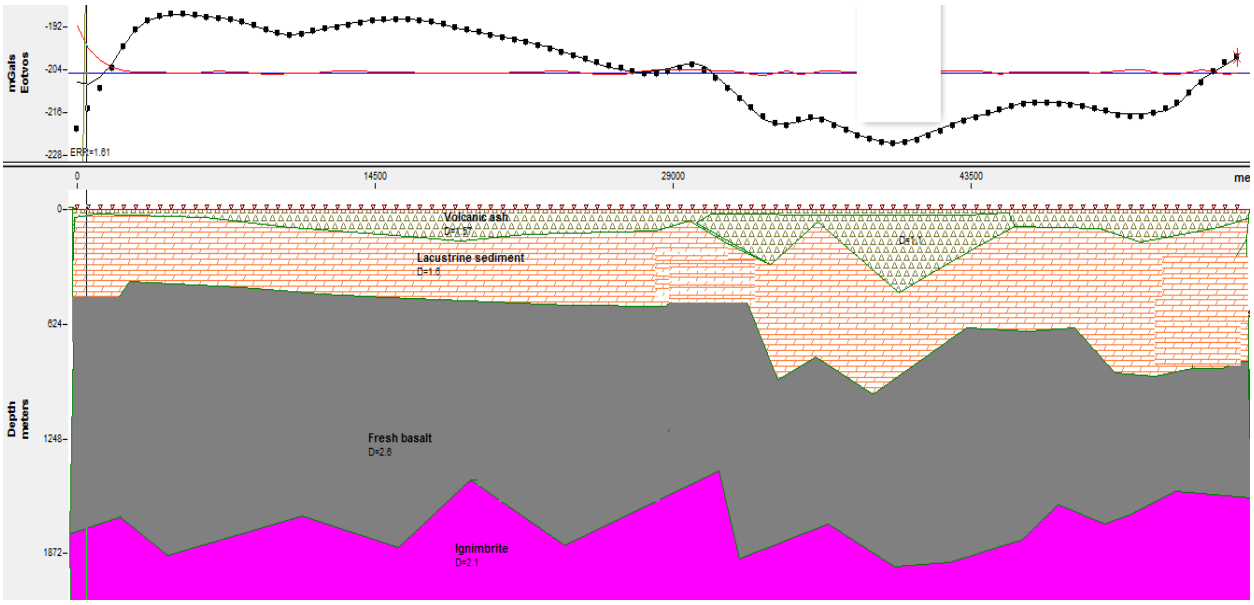

Figure 5.14 2D gravity anomaly map along profile two

The final gravity model corresponding to the first layer consists of relatively low density near surface volcanic ash products with an average density value of about 1.57 gm/cm^3 .The average thickness of this layer varies from 50m to 200 m. The second Layer has an average density value of 1.8 gm/cm^3 is interpreted as pleistocine – holocine lacustrine Sediment and underlain by Basalt rocks with an average thickness ranging from 550m to 1400m. The third layer shows thick fissural Basalt at the top of Aluto and thin Basalt deposit in the Aluto caldera. The fourth layer is interpreted as ignimbrite rocks overlain by Basalt rocks with an average thickness ranging from 1450m to 1900m.

The conclusion drawn based on a preliminary interpretation of the 2D gravity models is that:

A) Beneath the top of the Aluto volcanic complex, the thickness of low density volcanic ash (layer 1) deposit varies from 50-200m and the thickness of the lacustrine sediments (layer 2)

ranges from 450-500m. The thickness of the fissural basalt (layer 3) ranges from550m-1400m and the thickness of ignimbrite rock units (layer 4) are estimated to about 1900m.

B) Beneath the center of the Aluto complex (Aluto caldera) the thickness (about 200m) of low density volcanic ashes (layer 1) are thicker as compared to those residing the top parts of the volcano (Aluto ridge). The thickness of the Pleistocene - Holocene lacustrine sediments (layer 2) ranges from 250m-550m, thickness of the fissural basaltic rock (layer 3) deposit is estimated to about 500-550m and the thickness of ignimbrite rock (layer 4) is estimated to about 900m.

Beneath the Lake Langano, Lake Abijata and Lake Shala thickness of the volcanic ash products (layer 1) ranges from 50-200m. The thickness of the Pleistocene – Holocene lacustrine sediments (layer 2) ranges from 450-650m, thickness of the fissural basalt (layer 3) in these areas are estimated to about 650-1400m and the thickness of ignimbrite rock (layer 4) deposit is estimated to about 1350-1850m.

Investigation results based on the 2D gravity models indicate that the subsurface rock units in the study area constitute volcanic ash, lacustrine sediment, and Fissural basalt and ignimbrite rocks. The depth range of these rock units ranges from surface to 1900 m. Furthermore, the relatively high porosity and permeability of these rock units is thought to allow the flow of groundwater from Lake Langano towards Lakes Abijata and Lake Shala.

5.4.2 2D Magnetic model along profile P1

The 2D magnetic model is constructed using the GM-SYS modeling software. Any difference between the model response and the observed magnetic field are reduced by refining the model structure. It should be noted that magnetic models are non-unique, i.e. many Earth models can produce the same magnetic response, and similarly, several geological lithologies may be interpreted from a given model block's susceptibility properties.

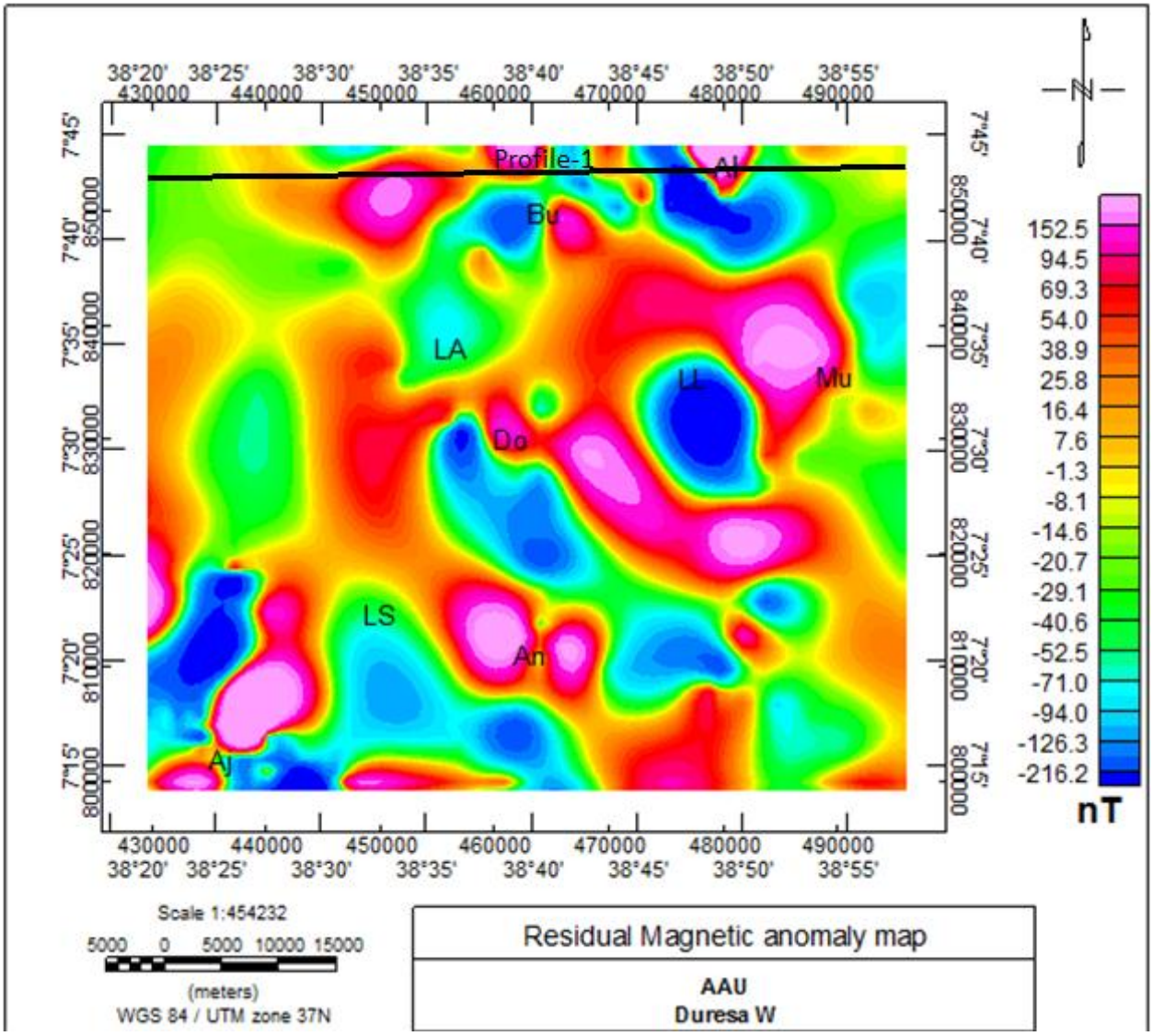

Figure 5.15: Residual magnetic anomaly map shows p-1

It is therefore important to use as many independent source of information as possible to constrain a model.

The magnetic model corresponding to the first layer consists of relatively low susceptibility near surface volcanic ash products with an average susceptibility value of about 0.001cgs

The average thickness of this layer varies from 120m to 280 m. The second Layer has an average magnetic susceptibility value of 0.003 is interpreted as Pleistocene – Holocene lacustrine Sediment and underlain by Fissural Basalt rocks with an average thickness ranging from 580m to 750m. The third layer shows thick fissural Basalt at the top of Aluto and thin Basalt deposit in

the Aluto caldera with an average thickness of 800m to 1450m. The fourth layer is interpreted as ignimbrite rocks overlain by Basalt rocks with an average thickness ranging from 1600m to 2300 m. Accordingly 2D magnetic modeling is developed along profile-1 from the residual magnetic map as shown in Figure 5.16. The developed model has an error of Err = 0.39.

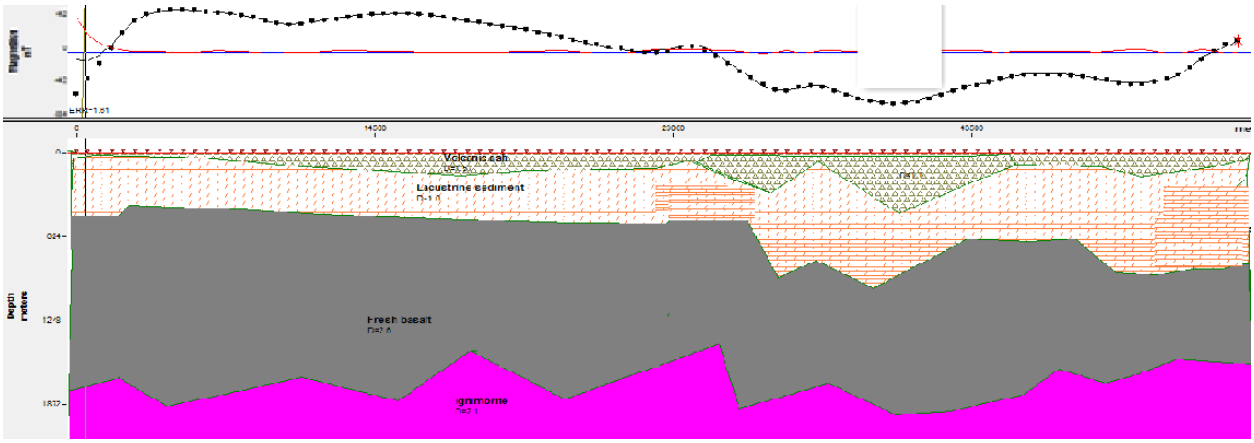

Figure 5.16: 2D Magnetic modeling of the study area

CHAPTER SIX

CONCLUSIONS AND RECCOMENDATIONS

6.1. Conclusions

Based on the results and interpretation dealt in the previous sections, the following conclusions can be drawn

The study area is characterized by relatively low Bouguer anomalies over both the northern and central part of the study area. The relatively high gravity values lie over the eastern, NE and SE of the study area. The minimum gravity anomalies coincide with the thick lacustrine sediment deposits in the northern shore of Lake Langano, Lake Abijita, Lake Shala and north western of Aluto volcanic center.

Comparison of regional and residual gravity and magnetic anomaly maps and enhancement techniques reveal that the volcanic complex centers (Aluto) and Shala caldera covered by high density gravity and magnetic anomaly are made correlated.

The N-S and NE-SW trending lineated subsurface geologic features (faults and fractures) revealed by both the horizontal gradient gravity map and the tilt derivative magnetic map are considered to be the major geologic structures that favor the flow of groundwater within Lake Langano towards Lake Abijita and Shala. This study has also determined that there are no east west lineated structures that favor the flow of groundwater from the three Lakes towards rift margin.

The interpretation of newly acquired magnetic and existing gravity and magnetic data give insight to map the subsurface structures contributing for groundwater flow at different locations ad depths in the study area. Based on our investigation results the intensity of gravity and magnetic fields are closely associated with the main lineated subsurface structural features.

6.2. Recommendations

The gravity data and magnetic data we have used are not sufficient to map the subsurface linear structures that control the flow of groundwater in the study area. Therefore, it is recommended to collect and fill the gap in the gravity and magnetic data coverage and acquire additional Electrical resistivity data to fully produce an integrated geophysical interpretation of the subsurface linear structures favoring groundwater flow in the Bulbula –Arsinegele rift corridor.

To understand and isolate the effect of deep and shallow sources using electrical resistivity method, it is recommended to collect VES data with a maximum AB/2 distance.

REFERENCES

Berhanu, B., Getachew, B., Tesfaye, T., Mohammed E., Tewoderos, G., and Aseres, H. (2011). A report on Aluto Gravity and Magnetic Surveys. EGS.

Berhe, S.M. (1978). Geological map (1:250,000) sheet NC37-15 (Nazret). Geological Survey of Ethiopia.

Boccaletti, M., Bonini, M., Mazzuoli, R., Abebe, B., Piccardi, L., Tortorici, L.(1998). Quaternary oblique extensional tectonics in the Ethiopian Rift (Horn of Africa).Tectonophysics 287, 97–116.

Bonini, M., Corti, G., Innocenti, F., Manetti, P., Mazzarini, F., Abebe, T. and Pecskay, Z. (2005). Evolution of the Main Ethiopian Rift in the frame of Afar and Kenya rifts propagation.

Chernet, T., W. K. Hart, J. L. Aronson, and R. C. Walter. (1998). New age constraints on the timing of volcanism and tectonism in the northern Main Ethiopian Rift–southern Afar transition zone (Ethiopia), J. Volcanol. Geotherm. Res., 80, 267–280, doi:10.1016/S0377 0273(97)00035-8

Corti, G. (2009). Continental rift evolution: from rift initiation to incipient break-up in the Main Ethiopian Rift, East Africa. «Earth Sci. Rev.»,96, 1-53.

Dentith, M. and Mudge, S.T. (2014). Geophysics for the Mineral exploration Geoscientist. Cambridge University Press, New York, USA.

Di Paola, G.M. (1972). The Ethiopian Rift Valley (between 7 and 8 40' lat. North). Bulletin

of Volcanology 36, 517–560.

Di Paola, G.M. (1976). Geological Map of the Tullu Moje ` Volcanic Area (Arusi: Ethiopian Rift valley). 1: 75,000 Scale. Laboratorio di Geocronologia e Geo- chimica isotopica, CNR, Pisa, Italy.

Di Paola, G.M., Seife, M.B., Arno, V. (1993). The Kella horst: Its origin and significance in crustal attenuation and magmatic processes in the Ethiopian Rift Valley. In: Geology and Mineral Resources of Somalia and Surrounding Regions, Ist. Agronom. Oltremare, Firenze, Relaz. Monograph. 113: 323 – 338.

Dobrin, M.B. and C.H. Savit. (1988). Introduction to Geophysical Prospecting, 4th Edition, McGraw-Hill, 1988.

Ebinger, C.J. and Sleep, N.H. (1998). Cenozoic magmatism in central and east Africa resulting from impact of one large plume. Nature, 395, 788–791.

Ebinger, C., 2005. Continental breakup**:** the East African perspective. Astronomy and Geoph. 46, 2.16–2.21.

Fairhead, J.D., K.J. Bennett, D.R.H. Gordon, and D. Huang (1994). Euler: Beyond the "Black Box", *SEG Expanded Abstr.* 13, 422-424.

FitzGerald, D., A. Reid, and P. McInerney (2004). New discrimination techniques for Euler deconvolution, *Comput. Geosci.* 30, 5, 461-469,

Foulger, G. R. and C. Peirce. (1876). Geophysical methods in geology.

Giday, W., Aronson, J.L. and Walter, R.C. (1990). Geology, Geochronology and Rift Basin Development in the central sector of the Main Ethiopian Rift. Geological Society of American Bulletin. 102: 439-458.

Hinze, W.J., VonFrese, R.B. and Saad, A.H. (2013). Gravity and Magnetic Exploration: Principles, Practices, and Applications. Cambridge University Press, New York, USA.

Hsu Shu-Kun (2002). Imaging magnetic sources using Euler's equation. *Geophysical prospecting*, 50, pp 15-25.

Huang, D., D., and K.A. Whaler (1995). Combined study of Euler's homogeneity equation for gravity and magnetic field, 57th Conf. and Tech. Exhib., Euro. Assoc., Expl. Geophys.

Hunegnaw, A.(1989). Gravity and electrical resistivity sounding applied in geothermal exploration in the northern part of the Main Ethiopian rift. University of Leicester.

Hoffman, C., Courtillot, V., Féraud, G., Rochette, P., Yirgu, G., Ketefo, E., Pik, R. (1997). Timing of the Ethiopian basalt event and implications for plume birth and global change. Nature 389, 838–841.

Huang, D., D. Gubbins, R.A. Clark, and K.A. Whaler (1995). Combined study of Euler's homogeneity equation for gravity and magnetic field, 57th Conf. and Tech. Exhib., Euro.

Assoc., Expl. Geophys, Extended abstracts, 144.

Kazmin, V., Berhe, S.M., Nicoletti, M. and Petrucciani, C. (1980). Evolution of the northern part of the Ethiopian rift. Atti Convegni Lincei, 47, 275–292.

Kearey, P., Brooks, M. and Hill, I. (2002). An introduction to Geophysical Exploration. Third edition. Black Well Science Ltd, Oxford, UK.

Klingele, E.E., I. Marson, and H.-G. Kahle (1991), Automatic interpretation of gravity

data in two dimensions: Vertical gradient, *Geophys. Prospect*. 39, 3, 407-434.

Lillie, R. J. (1999). Whole Earth Geophysics: An Introduction text to geologists and geophysicists. Prentice-Hall, Inc. Upper Saddle River, New Jersey, USA

Loke, M. H. (2001). Electrical imaging survey for environmental and engineering studies: A practical guide to 2D and 3D surveys.

Lowrie, W. (2007). Fundamental of Geophysics. Second edition. Cambridge University Press, New York, USA.

Milsom, J. and Eriksen, A. (2011). Field Geophysics. Fourth edition. John Wiley and Sons Ltd. West Sussex, UK.

Mohr, P. (1962). The Ethiopian Rift System. Bulletin of the Geophysical Observatory of Addis Ababa 5, 33–62.

Mohr, P., Zanettin, B. (1988). The Ethiopian food basalt province. In: Macdougall, J.D.

(Ed.), Continental flood basalts. Kluwer Academic Publishers, pp. 63–110.

Mussett, A.E and Khan, M.A. (2000). Looking in to the Earth: An introduction to Geological Geophysics. Cambridge University Press, USA.

Reynolds, J.M. (1997). An Introduction to Applied and Environmental Geophysics. John Wiley and Sons limited, England, UK. pp. 116-209, 415-522.

Saibi, H., Aboud, E. and Ehara, S. (2012). Analysis and interpretation of gravity data from the Aluto-Langano geothermal field of Ethiopia. Acta Geophysica, 60(2), pp.318-336.

Searl, R. and Gouin, P. (1972). A gravity Survey of the central part of the Ethiopian Rift Valley. East African Rifts. Tectonophysics, 15 (1/2): 41-52.

Phillips, J.D. (1998). Processing and interpretation of aeromagnetic data for the Santa Cruz Basin-Patahonia Mountains area, South-Central Arizona, U.S. Geological Survey Open-File Report, 02-98.

Telford, W.S., Geldart, L.P and Sheriff, R.E. (1990). Applied Geophysics. Second Edition Cambridge University Press, Cambridge, UK, pp 784.

Tibebu, A. (2001). Geophysical studies in the Aluto geothermal area. M.Sc. Thesis. Addis Ababa University.

Thompson, D.T. (1982). EULDPH: A new technique for making computer assisted depth estimates from magnetic data, *Geophysics*, 47: 31-37.

Tsegay, B. (2015). Integrated geophysical investigations at the Corbetti–Shala-Aluto segment of the main Ethiopian rift: implications for crustal structure, resource and volcanic hazards. M.Sc. Thesis. Addis Ababa University.

Ukstins, I.A., Renne, P.R., Wolfenden, E., Baker, J., Ayalew, D. and Menzies, M. (2002). Matching conjugate volcanic rifted margins: 40Ar/39Ar chrono-stratigraphy of pre- and syn-rift bimodal flood vol- canism in Ethiopia and Yemen. Earth Planet. Sci. Lett., 198, 289–306.